JEM Journal of Experimental Medicine

ARTICLE

Sensory neuron-immune cross talk tunes memory CD8⁺ T cell responses

Jiang Zhang[1], Timothy Y. Pan[1], Alexander L. Kley[1], Bharat Ashok Rajmalani[1], Jason B. Williams[1], Marine-Alexia Lefevre[1], Xiaopeng Fu[1], Qian Zhan[1], Liwen Deng[2], Yunlong Y. Jia[3], Kyle Deans[1], Yu Yan[1], Yunhao Zhai[4], Ozge Erdogan[2,5], Samantha Choi[2], Calvin Wong[2], Scott X. Atwood[3,6,7,8], Rachael A. Clark[1], Isaac M. Chiu[2], and Thomas S. Kupper[1]

Neuroimmune communication shapes antiviral immunity. The effect of pain signaling on vaccine-induced adaptive immunity, however, remains largely unexplored. We found that vaccinia virus (VACV) immunization by skin scarification (s.s.) activates transient receptor vanilloid 1 (Trpv1)⁺ sensory neurons, induces pain-like behaviors in mice, and promotes the release of the neuropeptide calcitonin gene-related peptide (CGRP) in the skin. Moreover, in the absence of Trpv1⁺ neurons, the memory CD8⁺ T cell response is significantly blunted. We further demonstrate that CGRP-Ramp1 signaling promotes Langerhans cell (LC) migration from the epidermis to draining LNs, thereby contributing to support antigen-specific CD8⁺ T cell responses and memory formation. Our findings reveal unexpected cross talk between sensory neurons, pain, LCs, and memory CD8⁺ T cells during VACV s.s. immunization, suggesting the potential to enhance CGRP-Ramp1 signaling for improving vaccine efficacy.

Introduction

Vaccines and immunization are a critical global health concern, as highlighted by the COVID-19 pandemic. Vaccinia virus (VACV) immunization using a bifurcated needle provides complete protection against variola major, the causative agent of smallpox, and a vaccination campaign based on this strategy led to the worldwide eradication of smallpox as a disease (Jacobs et al., 2009). However, vaccinations are not always this effective; for example, the effectiveness of the flu vaccine ranges from 40% to 60% (Frutos et al., 2025). Due to their convenience and accessibility, most vaccines are delivered into the hypodermis, which is a layer of fat and connective tissue just below the dermis or skeletal muscle, both with poorly characterized antigen-presenting cells (APCs). While readily accessible, skeletal muscle and adipose tissues are poorly adapted to initiate immune responses. Such s.c. or i.m. delivery bypasses the rich network of dendritic cells (DCs) and macrophages found in the epidermis and dermis (Malissen et al., 2014). Immunization through skin scarification (s.s.) generates superior T cell immunity and longer T cell memory against viral challenge (Liu et al., 2010; Jiang et al., 2012; Pan et al., 2021). Both the route of administration (s.s.) and the tissue-resident memory T (T_{RM}) cell response elicited by VACV may have jointly contributed to the success of the smallpox vaccine (Rotrosen and Kupper, 2023). However, s.s. is not universally embraced due to its imprecise nature and the discomfort it causes. Therefore, it is essential to elucidate the molecular and cellular mechanisms underlying s.s. that drive robust CD8⁺ T cell responses. Exploring alternative, more precise immunization strategies beyond s.s. could greatly enhance vaccine efficiency.

Molecular cross talk between the nervous and immune systems is integral to neurological function, barrier homeostasis, and host defense (Chu et al., 2020; Huh and Veiga-Fernandes, 2020), while its dysregulation can contribute to autoimmune diseases, cancer, and neurodegeneration (Pavlov and Tracey,

[1]Department of Dermatology and Harvard Skin Disease Research Center, Brigham and Women's Hospital, Harvard Medical School, Boston, MA, USA; [2]Department of Immunology, Harvard Medical School, Boston, MA, USA; [3]Department of Developmental and Cell Biology, University of California, Irvine, Irvine, CA, USA; [4]Wyss Institute for Biologically Inspired Engineering, Harvard University, Boston, MA, USA; [5]Department of Restorative Dentistry and Biomaterials Sciences, Harvard School of Dental Medicine, Boston, MA, USA; [6]NSF-Simons Center for Multiscale Cell Fate Research, University of California, Irvine, Irvine, CA, USA; [7]Center for Complex Biological Systems, Chao Family Comprehensive Cancer Center, University of California, Irvine, Irvine, CA, USA; [8]Department of Dermatology, University of California, Irvine, Irvine, CA, USA.

Correspondence to Thomas S. Kupper: tkupper@bwh.harvard.edu; Jiang Zhang: jzhang87@bwh.harvard.edu

J. Zhang's current affiliation is School of Medicine, The Chinese University of Hong Kong, Shenzhen, China. T.Y. Pan's current affiliation is Department of Biochemistry and Molecular Genetics, Northwestern University Feinberg School of Medicine, Chicago, IL, USA. A.L. Kley's current affiliation is Rutgers, The State University of New Jersey, New Brunswick, NJ, USA. M.-A. Lefevre's current affiliation is Centre International de Recherche en Infectiologie, University of Lyon 1 and École Normale Supérieure de Lyon, Inserm U1111, Lyon, France. X. Fu's current affiliation is BIDMC Center For Life Science, Boston, MA, USA. L. Deng's current affiliation is Rutgers New Jersey Medical School, Rutgers, The State University of New Jersey, Newark, NJ, USA. Y.Y. Jia's current affiliation is Centre de recherche en cancérologie de Toulouse, UMR 1037 INSERM, Toulouse, France. Y. Zhai's current affiliation is China Resources Research Institute of Life Sciences and Health Co., Ltd., Shenzhen, China. O. Erdogan's current affiliation is Boston University Henry M. Goldman School of Dental Medicine, Boston, MA, USA.

© 2026 Zhang et al. This article is distributed under the terms as described at https://rupress.org/pages/terms102024/.

Check for updates

Downloaded from rupress.org/jem/article-pdf/223/12/e20261215/2044247/jem_20261215.pdf by University of California Irvine user on 16 November 2026

2017; Shurin et al., 2020; Balood et al., 2022). The skin is innervated by an extensive network of low- and high-threshold sensory nerves, including nociceptive neurons specialized in detecting noxious stimuli and eliciting pain perception (Basbaum et al., 2009; Abraira and Ginty, 2013). Nociceptors can be activated through mechanical skin injury and other stimuli such as heat, cold, ultraviolet light, noxious chemicals, pathogen-derived ligands, or pH changes (Gouin et al., 2017; Cañedo-Dorantes and Cañedo-Ayala, 2019; Schmelz and Petersen, 2001). Upon activation, sensory nerve endings release mediators including neuropeptide calcitonin gene-related peptide (CGRP) into the tissues, which can act locally on innate and adaptive immune cells to modulate tissue immunity (Shurin et al., 2020; Deng et al., 2024; Roger et al., 2022; Wang et al., 2024). Nociceptor neurons have been found to be important in regulating both the initiation of innate immunity and the primary effector phases of adaptive immune responses to virus infection (Filtjens et al., 2021; Wu et al., 2024). While sensory neurons have been implicated in regulating primary antiviral T cell responses (Filtjens et al., 2021), their role in shaping antiviral CD8⁺ T cell memory remains poorly defined. Our research aims to uncover how neuro-immune cross talk influences the generation of long-lasting T cell memory in response to immunization by s.s. and how targeting this neuro-immune cross talk could optimize vaccination efficiency.

Here, we find that VACV exposure via s.s. induces robust pain through transient receptor vanilloid 1 (Trpv1)⁺ sensory neurons, whose activation triggers the release of the neuropeptide CGRP in the skin. CGRP signaling through its receptor component Ramp1 further facilitates Langerhans cell (LC) migration to the draining LNs (dLNs), thereby contributing to the generation of memory CD8⁺ T cell responses. Moreover, intradermal treatment of a CGRP agonist enhances memory CD8⁺ T cell accumulation, while the CGRP antagonist (CGRP8-37) impairs this response. Our findings uncover a novel role for sensory neurons in regulating the memory CD8⁺ T cell response to viral infection and identify CGRP as a promising candidate for vaccine development.

Results

Skin scarification induces pain and promotes CGRP release from sensory neurons

The nervous and immune systems, traditionally viewed as independent entities, are increasingly recognized as interconnected networks that communicate through a complex web of signaling molecules (Deng et al., 2024; Roger et al., 2022; Wang et al., 2024). Neurons release neurotransmitters and neuropeptides that modulate the activity of immune cells. Trpv1 is a ligand-gated ion channel that detects capsaicin and noxious heat and is expressed by many dorsal root ganglion (DRG) neurons, including peptidergic nociceptors that express CGRP (Achanta et al., 2018; Zhang et al., 2020; Pinho-Ribeiro et al., 2018). Activated Trpv1⁺ neurons can release CGRP or substance P (SP) in response to different pathogen exposures (Chiu et al., 2013; Cohen et al., 2019; Kashem et al., 2015; Pinho-Ribeiro et al., 2018; Serhan et al., 2019; Perner et al., 2020; Wang et al., 2025). Given our observation that s.s. can induce superior CD8⁺ T cell responses to VACV compared with other immunization routes (Liu et al., 2010; Pan et al., 2021) and the abundance of nociceptor nerve fibers in the skin that can release neuropeptides (Chiu et al., 2013; Blake et al., 2019), we hypothesize that s.s. with VACV virus causes pain by activating sensory neurons, thus promoting neuropeptide release and modulating the memory CD8⁺ T cell response.

To determine whether vaccinia vaccination through s.s. induces neuropeptide release at the immunization site, we utilized an ex vivo organ culture of skin explants (Pinho-Ribeiro et al., 2018) from mice at different time points postimmunization (p.i.) (Fig. 1 A). Skin explant cultures allow assessment of CGRP released into the extracellular space following nociceptor activation, enabling comparison of CGRP dynamics between experimental conditions. The levels of the neuropeptide CGRP in the skin peaked between 6 and 24 h p.i. and diminished thereafter (Fig. 1 B). In contrast, no significant changes were observed in the levels of SP, another neuropeptide, during these same time points (Fig. 1 B).

To study the nature of pain caused by VACV s.s., we established a VACV infection model of the mouse hindpaw, which allows measurement of reflexive pain behaviors, and tested these behaviors for up to 28 days. VACV s.s. induced an increased mechanical allodynia (as measured by von Frey filaments [Pinho-Ribeiro et al., 2018]) as early as 2 h p.i., which peaked at 6 h p.i. and persisted through 48–72 h p.i. (Fig. 1 C and Fig. S1 A). A secondary peak in mechanical sensitivity was observed at day 5 that resolved by day 21 (Fig. S1 A). Consistent with the mechanical hypersensitivity detected by von Frey testing, mice immunized with VACV via s.s. also exhibited significantly reduced paw withdrawal latencies to heat stimuli using the Hargreaves assay, indicating enhanced thermal nociception (Fig. 1 D). A modest secondary increase in thermal sensitivity was also observed at day 5 p.i. (Fig. S1 B). Tissue swelling kinetics were also quantified, showing a correlation with pain, with an immediate swelling peak at 6 h p.i. that persisted through 72 h p.i., followed by a secondary peak at 96 h (Fig. 1 E and Fig. S1 C).

Unlike the more rapid and robust response induced by s.s., s.c. injection of VACV elicited only a modest and delayed increase in cutaneous CGRP levels, which was most evident at 24 h p.i. and subsequently declined (Fig. 1 F). In contrast, VACV administered by s.s. induced a pronounced early peak in CGRP release at 6 h p.i., indicating distinct kinetics and magnitude of sensory neuronal activation between the two routes (Fig. 1 F). To further investigate the contribution of mechanical injury to this early response, we compared s.s. alone with VACV administered by s.s. At day 1 p.i., scarification alone was sufficient to increase CGRP release, whereas the addition of VACV did not further enhance CGRP levels (Fig. S1 D), suggesting that CGRP release is largely driven by the mechanical injury associated with scarification. To determine whether the second phase of mechanical sensitivity observed on day 5 reflects a prolonged effect of s.s. or is driven by viral infection, we compared mice subjected to scarification alone with mice receiving VACV scarification at the same time point. We found no difference in CGRP levels between

Downloaded from rupress.org/jem/article-pdf/223/12/e20261215/2044247/jem_20261215.pdf by University of California Irvine user on 16 November 2026

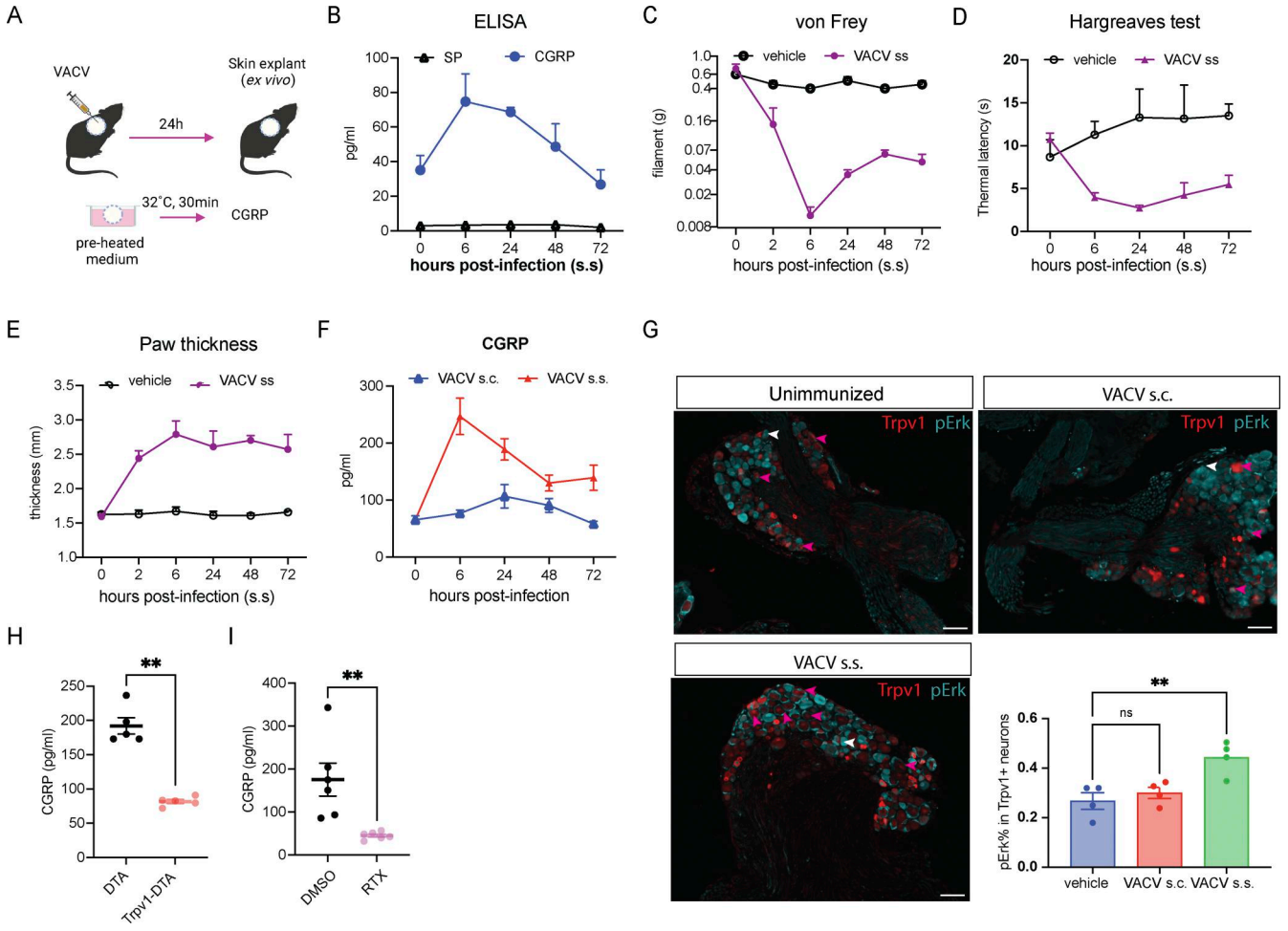

Figure 1. **Skin scarification induces pain and promotes CGRP release from sensory neurons. (A)** Measurement of CGRP/SP release ex vivo and analysis of CGRP/SP levels from 12 mm skin punch biopsies. Mice were infected with VACV through different routes (s.c. or s.s.). Skin samples were collected at specific time points, incubated in 0.5 ml DMEM for 30 min in a 32°C shaking incubator (150 rpm), after which bath supernatants were collected and analyzed for CGRP/SP levels. **(B)** CGRP/SP release from VACV-infected skin (s.s.) at various time points after infection. *N* = 3 mice in each group from one experiment. **(C–E)** s.s. on mouse hindpaw (VACV s.s.) induces (C) mechanical hypersensitivity measured using Von Frey filaments. *N* = 4 mice per group; data are representative of two independent experiments. **(D and E)** Thermal hypersensitivity measured using the (D) Hargreaves test and (E) tissue swelling observed following VACV s.s. *N* = 4 per group; data are representative of two independent experiments. **(F)** CGRP release from infected skin via s.c. or s.s. at different time points after infection. *N* = 4 mice per group; data are representative of two independent experiments. **(G)** Representative images of pERK expression in cervical and thoracic DRG neurons from untreated mice or mice following VACV immunization of the upper dorsal skin. Sections were stained for βIII-tubulin (green), pERK (cyan), and TRPV1 (red). Scale bar = 50 µm. Quantification of the percentage of pERK⁺ neurons among Trpv1⁺ DRG neurons following VACV delivery by the indicated routes. Four mice were analyzed per group, with two to three DRG sections examined per mouse. pERK⁺ neurons were manually counted in each section. **(H and I)** CGRP release from the skin of (H) *DTA* versus *Trpv1-DTA* mice or (I) DMSO- versus RTX-treated mice. *N* = 5 mice per group from one experiment. Mann–Whitney test (H and I) was used for statistical comparisons, with significance denoted as **P < 0.01. Error bars represent mean ± SEM. **(A)** Figure adapted from an image created in BioRender.

naïve mice and scarification-only controls at day 5 (Fig. S1 E). In contrast, CGRP levels were significantly increased in VACV s.s. mice compared with scarification-only mice (Fig. S1 E). The CGRP peak observed at day 5 was not induced by scarification alone and coincided with maximal tissue swelling, suggesting that VACV-driven inflammatory signals might promote a second phase of nociceptor activation (Baral et al., 2019) that requires further investigation.

We next examined the effect of virus infection on sensory neuron activation using phosphorylated ERK (pERK) as a marker of primary DRG neuron activation (Gao and Ji, 2009). Because VACV skin immunization was performed on the upper dorsal skin, cervical and thoracic DRGs were collected to sample sensory neurons innervating the anatomical region encompassing the immunization site. VACV infection delivered via s.s. induced a robust increase in the number of pERK-positive cells among Trpv1⁺ neurons in DRGs at 24 h p.i., indicating nociceptor activation (Fig. 1 G). In contrast, VACV administration via s.c. infection failed to elicit comparable pERK induction (Fig. 1 G). These results demonstrate that sensory neuron activation in response to VACV is route-dependent and preferentially triggered by s.s.

To assess the role of these Trpv1⁺ neurons in VACV immunization, we bred Trpv1-Cre/diphtheria toxin (DT) A

Downloaded from rupress.org/jem/article-pdf/223/12/e20261215/2044247/jem_20261215.pdf by University of California Irvine user on 16 November 2026

(*Trpv1-DTA*) mice to specifically ablate Trpv1-lineage nociceptors (Mishra and Hoon, 2010; Mishra et al., 2011). *Trpv1-DTA* mice showed a significant reduction in CGRP levels in both skin biopsies and DRG upon VACV s.s. compared with Cre$^-$/DTA$^+$ littermate controls (Fig. 1 H and Fig. S1 F). Mice were also treated with resiniferatoxin (RTX), a high-affinity Trpv1 agonist, which induces chemical ablation of Trpv1$^+$ neurons and their nerve fibers (Mishra and Hoon, 2010; Tender et al., 2005). RTX-treated mice also showed decreased CGRP levels upon VACV s.s. compared with vehicle-treated control mice (Fig. 1 I). However, CGRP levels were reduced but not completely eliminated in *Trpv1-DTA* and RTX-treated mice, indicating that Trpv1$^+$ nociceptors constitute the dominant but not exclusive source of CGRP in this setting. Importantly, in *Trpv1-DTA* mice, total pERK induction within βIII-tubulin$^+$ sensory neurons was not significantly reduced compared with controls (Fig. S1, G and H), indicating that although Trpv1$^+$ neurons are selectively activated by s.s., other non-Trpv1$^+$ sensory neuron populations can also be engaged during infection.

We next examined the cellular sources of CGRP and the extent to which Trpv1$^+$ nociceptors account for CGRP production in this model. Immunofluorescence analysis of DRG revealed that the majority of CGRP$^+$ neurons co-expressed Trpv1, with the majority (>85%) of CGRP$^+$ cells being Trpv1$^+$, while a smaller fraction represented Trpv1$^-$CGRP$^+$ neurons (Fig. S1, I and J). This distribution is consistent with transcriptional profiling of sensory neuron subsets (MouseBrain.org) and with prior reports demonstrating partial preservation of CGRP following Trpv1-targeted ablation (Mishra et al., 2011).

We also determined whether Trpv1$^+$ neurons are necessary for pain induced by VACV infection through s.s. Mechanical hypersensitivity after VACV infection was abolished in RTX-treated mice in the first 72 h, indicating that Trpv1$^+$ neurons are the major cell type mediating the pain at early time points (Fig. S1 K). However, the second phase of pain-like behaviors did not differ between vehicle and RTX-treated groups in terms of mechanical sensitivity by the von Frey assay (Fig. S1 K). In contrast, thermal nociception assessed by the Hargreaves test was significantly reduced in RTX-treated mice compared with vehicle controls at both early and late time points (Fig. S1 L), indicating a sustained requirement for Trpv1$^+$ neurons in mediating heat-evoked pain responses. Furthermore, paw thickness changes did not differ between the two groups (Fig. S1 M). These data indicate that while Trpv1$^+$ neurons mediate mechanical and heat pain during the early scarification process, the later phase of pain sensitivity, especially mechanical hypersensitivity, involves the activation of other sensory neuron populations.

Taken together, these data demonstrate that s.s. induces pain-like behaviors and promotes CGRP release in the skin and that genetic or chemical ablation of Trpv1$^+$ neurons significantly impairs CGRP release following VACV infection, particularly at the early time point.

Trpv1$^+$ neurons are required for antigen-specific CD8 T cell responses

We next determined whether Trpv1-expressing neurons influence the generation of T cell memory. To evaluate the T cell response to s.s. and vaccination, we used the OT-I system, where OT-I T cells express a transgenic TCR specific for an H-2Kb–restricted epitope in OVA, residues 257–264 (Liu et al., 2010). OT-I T cells were transferred retro-orbitally into *Trpv1-DTA* mice or control mice 1 day before immunization with VACV encoding OVA$^{257–264}$ (VACV-OVA) through s.s. (Liu et al., 2010) (Fig. 2 A). No difference in OT-I T cell numbers or percentages was found in the skin dLNs or in the spleen (Fig. S2, B and C). By contrast, significantly lower OT-I T cell numbers were found in the skin of *Trpv1-DTA* mice compared with *DTA* control mice at day 7 p.i. (Fig. S2 D). Similar to *Trpv1-DTA* mice, mice treated with RTX to chemically ablate Trpv1$^+$ neurons also showed an impaired CD8$^+$ T cell response compared with vehicle-treated mice, as evidenced by reduced OT-I T cell numbers in the skin (Fig. S2 E), while not differing in the dLNs or spleen at day 7 p.i. (Fig. S2, F and G).

Beyond the primary effector phase, total memory CD8$^+$ T cells and OT-I T cells were assessed at >28 days p.i. A reduced number of OT-I T cells was observed in the dLNs of Trpv1$^+$ neuron-ablated mice (*Trpv1-DTA* and RTX-treated mice) compared with the control groups (Fig. 2, B, C, E, and F). However, no significant differences in total OT-I T cell numbers were detected in the skin (Fig. 2, D and G). Next, we assessed the phenotype of skin OT-I T cells using CD69 and CD103, which are used as markers of skin T_{RM} cells (Mackay et al., 2013). Using these criteria, we found that more than 90% of skin OTI are CD69$^+$ and/or CD103$^+$. However, we did not observe differences in the CD69$^+$CD103$^+$ population between *DTA* and *Trpv1-DTA* groups (Fig. 2, H and I) or between control and RTX-treated groups (Fig. 2, J and K). These data suggest that Trpv1-expressing neurons are necessary to generate memory T cells in dLNs upon VACV immunization through s.s., but do not necessarily affect memory cells in the skin niche.

The CGRP-Ramp1 signaling axis regulates memory T cell generation upon VACV infection

To test the requirement of CGRP signaling, we compared CGRP receptor Ramp1-deficient (*Ramp$^{-/-}$*) and control (*Ramp1$^{+/+}$*) mice after VACV s.s. At >28 days p.i., OT-I T cell numbers were much lower in the LN of *Ramp1$^{-/-}$* mice than in their control littermates (Fig. 3 A), demonstrating that CGRP-Ramp1 signaling is required to elicit robust memory CD8 T cell expansion during VACV s.s. infection. We have previously reported that VACV delivery via s.s. provides better protection against cutaneous challenge than other delivery routes, including s.c., i.d., and i.m. routes (Liu et al., 2010; Jiang et al., 2012). To evaluate the role of nociceptor neurons in viral clearance, we challenged mice previously immunized with VACV (VACV memory mice) with a secondary VACV-WR infection to the skin and measured viral load at the challenge site 3 days later. *Ramp1$^{-/-}$* mice showed reduced efficiency in clearing virus from the infected site compared with *Ramp1$^{+/+}$* mice (Fig. 3 B). These data indicate significant impairment in T cell memory in *Ramp1$^{-/-}$* mice. Therefore, we next investigated whether chemical stimulation or inhibition of CGRP-Ramp1 signaling could fine-tune the T cell memory response.

To this end, we infected WT mice with VACV s.c. or through s.s., and simultaneously treated them intradermally with CGRP

Downloaded from rupress.org/jem/article-pdf/223/12/e20261215/2044247/jem_20261215.pdf by University of California Irvine user on 16 November 2026

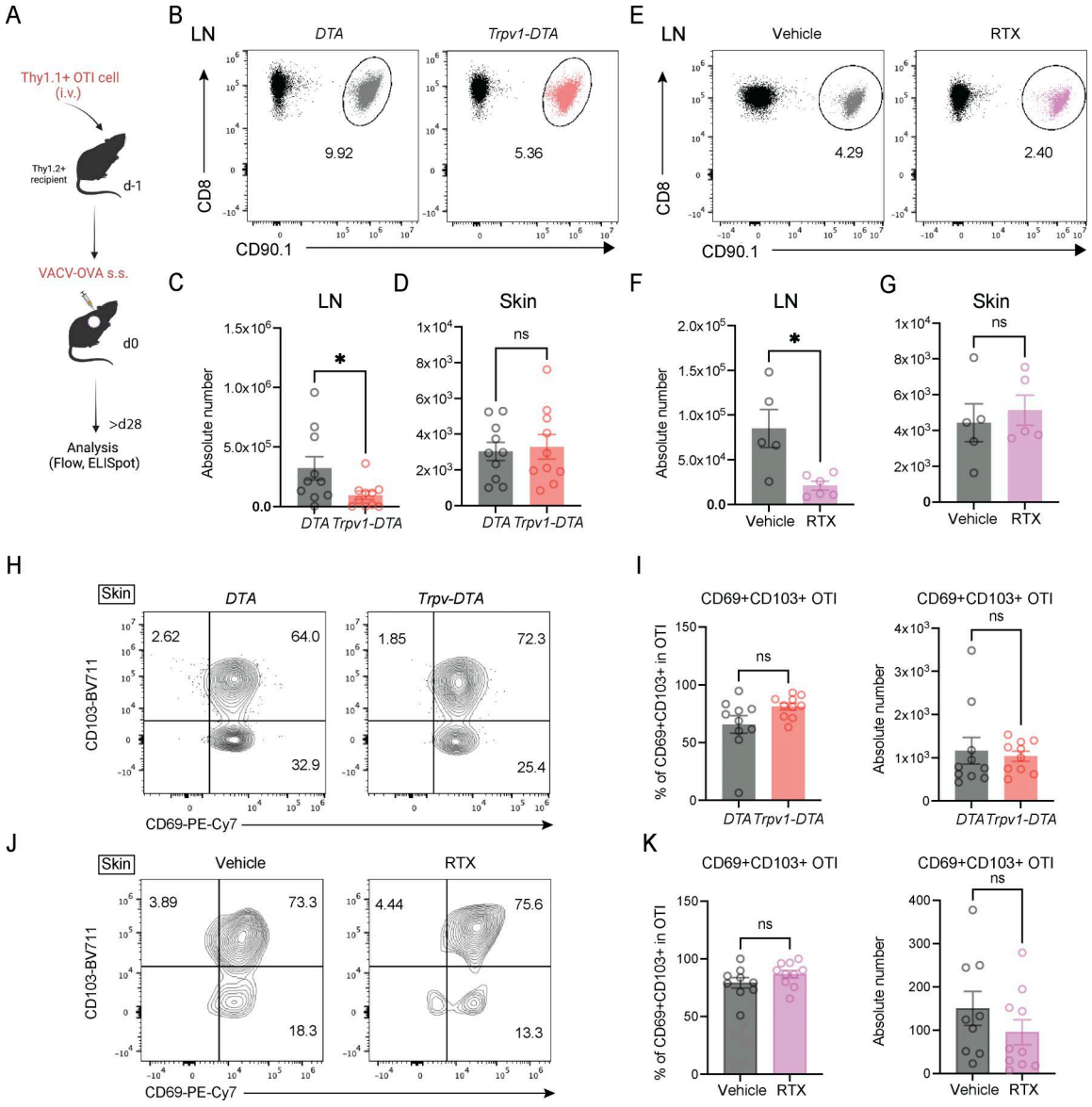

Figure 2. **Nociceptor neurons are required to promote a memory CD8 T cell response to VACV infection. (A)** Experimental design used for monitoring antiviral CD8 T cell response in vivo. Thy1.2$^+$ recipient mice were transferred with naïve Thy1.1$^+$ OT-I cells 1 day prior to VACV-OVA infection by s.s. **(B and E)** 4 wk later, flow cytometry was performed to analyze OT-I (CD8$^+$CD90.1$^+$) T cells of dLNs in DTA versus Trpv1-DTA mice (B) and DMSO-treated versus RTX-treated mice (E). **(C, D, F, and G)** Quantification of OT-I T cells in dLNs and 12 mm punch skin samples. Data in C and D are from *n* = 10 mice per group, pooled from two independent experiments; data in D and F are from *n* = 5 mice per group, representative of two independent experiments. **(H)** Representative flow cytometry plots showing CD69$^+$CD103$^+$ populations gating on total memory OTI T cells in skin from control (DTA) and nociceptor-deficient (Trpv1-DTA) mice. **(I)** Quantification of the frequency and absolute number of CD69$^+$CD103$^+$ OTI T cells. *N* = 9–10 mice per group pooled from two independent experiments. **(J)** Representative flow cytometry plots showing CD69$^+$CD103$^+$ populations gated on total OTI T cells in skin from vehicle- and RTX-treated mice. *N* = 9–10 mice per group, representative of two independent experiments. **(K)** Quantification of the frequency and absolute number of CD69$^+$CD103$^+$ OTI T cells in the skin of vehicle- and RTX-treated mice. Mann–Whitney test (C, D, F, G, I, and K) was used for statistical comparisons, with significance denoted as *P < 0.05 and "ns" indicating not significant. Error bars represent mean ± SEM. **(A)** Figure adapted from an image created in BioRender.

agonist CGRPα (the main isoform of the neuropeptide in nociceptors) or the CGRP receptor antagonist, CGRP8-37, at both the primary effector (Fig. S3 A) and memory phases (Fig. 3 C). Strikingly, CGRPα-treated mice exhibited increased OT-I T cell numbers in the skin at both day 6 p.i. (Fig. S3 B) and day 28 p.i. (Fig. 3 D). Conversely, treatment with the CGRP receptor antagonist resulted in attenuated cutaneous CD8 T cell responses, most notably reflected by a reduction in absolute OTI T cell numbers (Fig. 3 E and Fig. S3 C). A similar effect was observed in the LN at day 6 p.i., though to a lesser degree (Fig. S3, D and E). We also detected a higher number of memory OT-I T cells in the dLN of the CGRPα-treated group (Fig. 3 F) and a trend toward a lower number of total memory OT-I T cells in CGRP8-37–treated group compared with the control (Fig. 3 G). Notably, CGRP-dependent effects are most apparent in the skin during the primary response and become more evident in the dLNs during

Downloaded from rupress.org/jem/article-pdf/223/12/e20261215/2044247/jem_20261215.pdf by University of California Irvine user on 16 November 2026

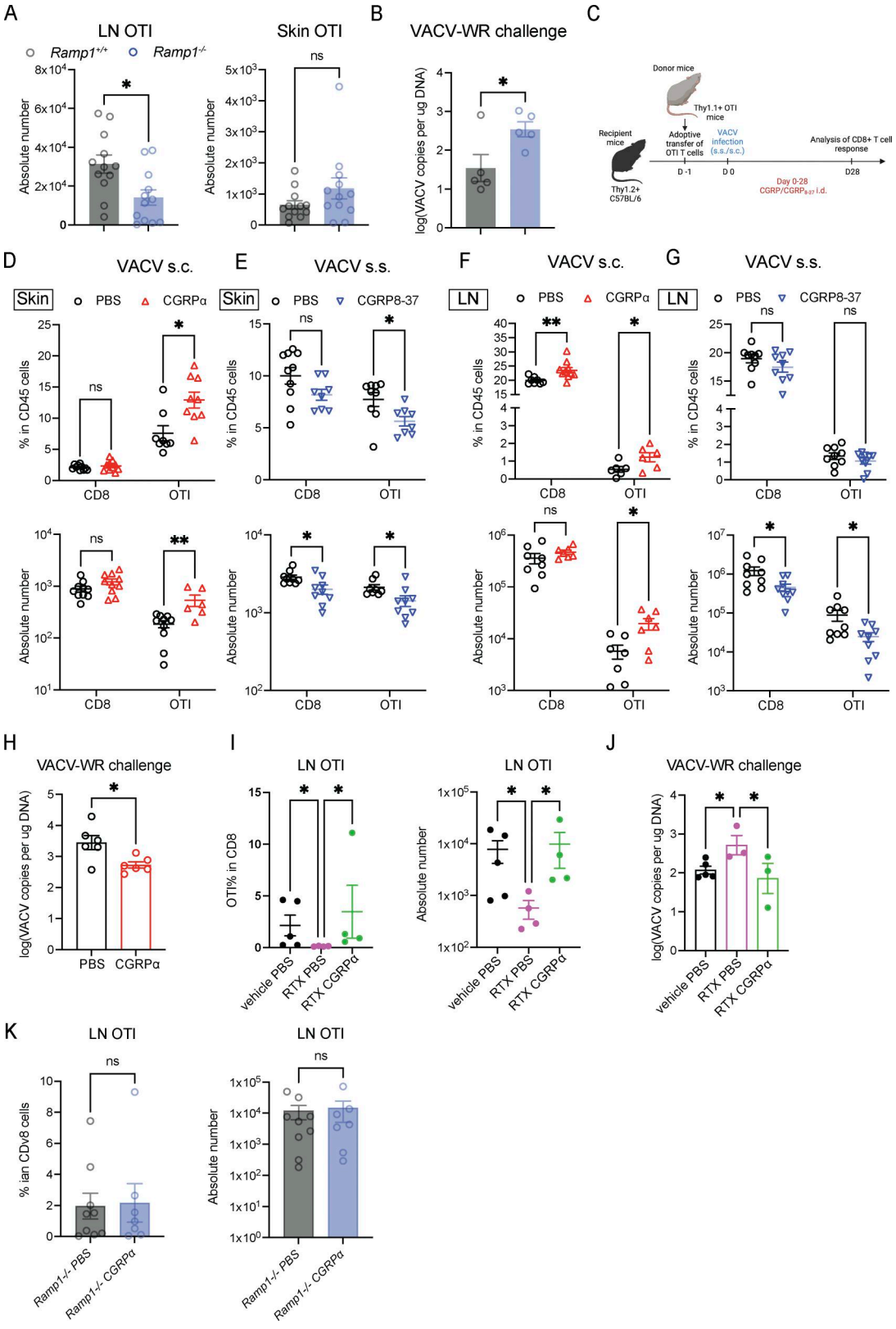

Figure 3. **CGRP agonist promotes virus-specific CD8 T cell generation following skin VACV infection. (A)** Naïve Thy1.1⁺ OT-I cells were transferred into Thy1.2⁺ *Ramp1*$^{+/+}$ and *Ramp1*$^{-/-}$ mice 1 day before infection with VACV-OVA via s.s. 4 wk later, OT-I T cell numbers in the LN or skin were quantified by flow cytometry using beads. *N* = 12 mice per group; data are pooled from three independent experiments. **(B)** 4 wk after VACV-OVA immunization, mice were challenged with VACV-WR (2×10^6 pfu) at the same skin site. 3 days later, the skin biopsies were collected, and DNA was extracted for quantitative PCR to quantify the viral load of each sample. *N* = 5 mice per group, representative of two independent experiments. **(C)** Experimental design to determine the effect of the antagonist CGRP8-37 injection on memory CD8⁺ T cell response. Naïve Thy1.1⁺ OT-I cells were transferred into Thy1.2⁺ B6 mice 1 day before infection with

Downloaded from rupress.org/jem/article-pdf/223/12/e20261215/2044247/jem_20261215.pdf by University of California Irvine user on 16 November 2026

VACV-OVA via s.c. route or s.s. Mice were given daily injections of CGRPα or CGRP8-37 for the first 6 days p.i., followed by injections every other day until day 28. **(D–G)** Skin (D and E) and LN (F and G) samples from treated and vehicle control groups were collected at day 28 for flow cytometry analysis. Data in D–G are from *n* = 7–9 mice per group pooled from two independent experiments. **(H)** Following VACV-OVA s.c. immunization, PBS or CGRPα was administered for 28 days using the same treatment schedule as in C. At 4 wk p.i., mice were challenged with VACV-WR (2×10^6 pfu) at the same skin site. 3 days after challenge, the skin biopsies were collected, and DNA was extracted for quantitative PCR to quantify the viral load of each sample. **(I)** Antigen-specific $CD8^+$ T cell (OTI T cell) percentages and numbers at day 28 p.i. in dLNs of RTX-treated mice with or without CGRPα administration. *N* = 4–5 mice per group from one experiment. **(J)** Viral load in skin following 3 days of VACV-WR rechallenge in vehicle- or RTX-treated mice with or without CGRP treatment. *N* = 3–5 mice per group from one experiment. **(K)** Quantification of OT-I T cell responses in dLNs of *Ramp1*$^{-/-}$ mice at day 28 following VACV-OVA s.c. immunization and treatment with PBS or CGRPα using the same treatment schedule as in C. *N* = 7–9 mice per group from one experiment. Multiple Mann–Whitney tests (A, B, D, E–H, and K) and Kruskal–Wallis test (I and J) were used for statistical comparisons, with significance denoted as *P < 0.05, **P < 0.01, and "ns" indicating not significant. Error bars represent mean ± SEM. **(C)** Figure adapted from an image created in BioRender.

the memory phase, mirroring the phenotype observed in nociceptor-ablated mice. To further assess whether CGRP signaling functionally enhances recall responses, we performed an additional rechallenge experiment in which mice were re-infected with VACV-WR at day 28 p.i. in the presence or absence of CGRPα treatment. In this setting, CGRPα-treated mice exhibited a significantly enhanced capacity to clear the virus compared with control mice (Fig. 3 H). This functional improvement upon secondary challenge supports a role for CGRP signaling in promoting effective memory $CD8^+$ T cell recall responses, rather than merely augmenting early priming.

To directly test whether the defect in $CD8^+$ T cell responses observed in neuron-ablated mice could be dissociated from nociception and attributed to loss of neuropeptide signaling, we administered exogenous CGRPα to RTX-treated mice. Under these conditions, CGRPα treatment rescued the impaired memory $CD8^+$ T cell response, restoring antigen-specific $CD8^+$ T cell numbers in the dLNs (Fig. 3 I). In addition, we performed a skin rechallenge assay and found that CGRP administration also restored the defective viral clearance observed in RTX-treated mice (Fig. 3 J). Consistent with this finding, CGRPα administration in *Ramp1*$^{-/-}$ mice did not enhance OT-I T cell responses in dLNs (Fig. 3 K). Together, these results demonstrate that CGRP signaling is sufficient to compensate for nociceptor ablation and support the conclusion that the absence of neuropeptide signaling underlies the impaired antiviral immunity.

Using surface markers CD44 and CD62L, we further categorized OT-I T cells from dLNs into central memory T cells (T_{CM}, $CD44^+CD62L^+$) and effector memory T cells (T_{EM}, $CD44^+CD62L^-$). We observed that the T_{CM} population, rather than T_{EM}, was affected by CGRPα or CGPR8-37 treatment (Fig. 4, A–D). To complement these findings and determine whether sensory neuronal input influences the functional quality of the resulting memory $CD8^+$ T cells, we next assessed OT-I T cell functions following RTX-mediated depletion of $Trpv1^+$ sensory neurons. In our model, RTX treatment markedly reduces sensory neuron-derived CGRP release following VACV s.s. (Fig. 1 I), providing a functional connection between $Trpv1^+$ sensory neurons and downstream CGRP signaling. Upon ex vivo cognate peptide re-stimulation, T_{CM} cells isolated from RTX-treated mice displayed a significantly diminished capacity to produce granzyme A (GzmA), IFN-γ, and TNF-α compared with T_{CM} cells from vehicle-treated mice (Fig. 4, E and F). These findings indicate that T_{CM} cells generated in the absence of nociceptor neurons are functionally compromised.

Both circulating, VACV-specific effector memory T cells and skin-resident memory T cells (T_{RM}) are generated following VACV s.s. immunization at the memory phase (Jiang et al., 2012; Pan et al., 2021; Liu et al., 2010). Given that T_{CM} cell numbers in the dLNs were altered upon CGRPα stimulation while skin T_{RM} remained unchanged (Figs. 3 and 4), we next sought to evaluate the relative contribution of central memory cells during recall responses. We rechallenged the immunized mice with VACV-WR and treated the mice with FTY720 at day −1 and day 1 p.i. to block lymphocyte egress from LNs and thereby prevent recruitment of circulating T_{CM} cells. Under this condition, mice exhibited a significantly reduced capacity to clear viral infection 3 days after rechallenge (Fig. S3, F and G), despite the persistence of skin T_{RM} cells. These findings indicate that circulating memory T cells contribute substantially to the recall response and efficient control of viral infection. While skin T_{RM} cells may participate in the early detection of local antigen re-encounter and initiation of recall responses, our data do not directly address their precise functional role in this process. Together, our findings are consistent with a model in which T_{RM} cells function as local sentinels that rapidly detect antigen and initiate immune activation, while T_{CM} cells may be required to sustain and amplify systemic recall responses necessary for efficient pathogen clearance. This "T_{RM} alarm" likely facilitates the recruitment of T_{CM} from the LNs to combat the viral infection effectively.

CGRP-Ramp1 signaling is required for LC migration following VACV infection

Our preliminary data reveal that the rapid and massive release of CGRP into the skin following VACV s.s. enhances antigen-specific CD8 T cell responses at both primary and memory stages during viral infection. However, the role of CGRP-Ramp1 signaling in CD8 T cell responses in the skin remained unclear.

The CGRP receptor Ramp1 is broadly expressed throughout skin immune cells, with particularly higher expression in monocytes, lymphocytes, and mesenchymal cells based on the Human-Mouse skin database (Fig. S3, H and I) (Thrane et al., 2023). DCs, essential APCs for T cell priming, have been established to colocalize with sensory neurons and respond to neuropeptides, which polarize their cytokine production (Kashem et al., 2015), migration (Perner et al., 2020), and priming (Filtjens et al., 2021). We, therefore, analyzed the DC response in nociceptor-deficient and -sufficient mice on day 3 p.i. dLN cells were isolated from infected *Trpv1-DTA* and *DTA* control mice and were analyzed by flow cytometry. We were able to distinguish

Downloaded from rupress.org/jem/article-pdf/223/12/e20261215/2044247/jem_20261215.pdf by University of California Irvine user on 16 November 2026

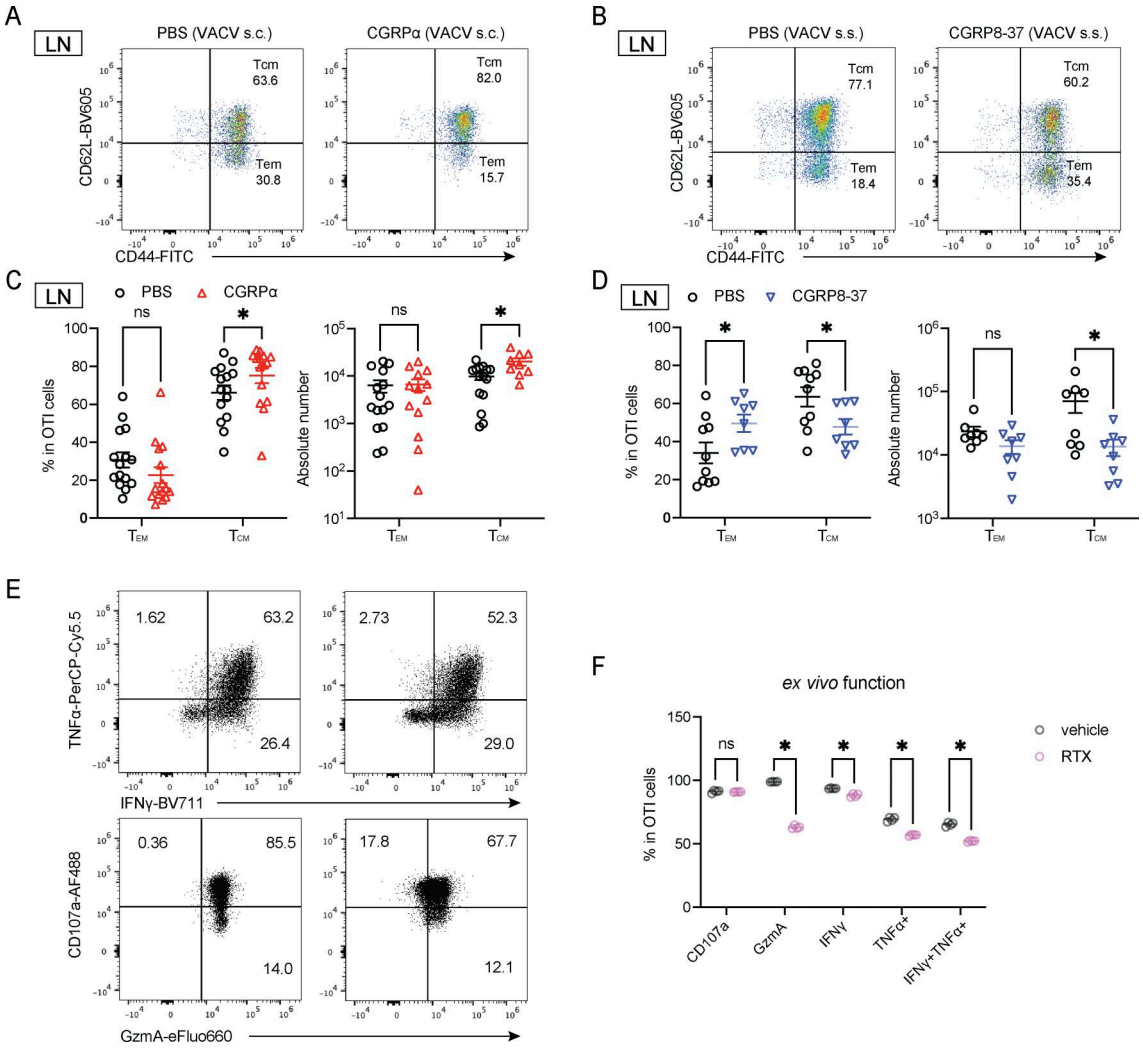

Figure 4. **CGRP signaling promotes OT-I central memory formation and supports memory CD8⁺ T cell effector functions. (A and B)** Representative flow cytometry plots showing T_{CM} ($CD44^+CD62L^+$) and T_{EM} ($CD44^+CD62L^-$) populations gated on total OT-I T cells in LNs from mice treated with either (A) CGRPα or (B) CGRP8-37. **(C and D)** Quantification of the frequency and absolute number of T_{CM} and T_{EM} across different treatment groups. Data in C are from $n = 9–15$ mice per group pooled from two independent experiments; data in D are from $n = 8–10$ mice per group representative of two independent experiments. **(E and F)** Vehicle- or RTX-treated mice were adoptively transferred with OTI cells and immunized with VACV-OVA. 8 wk later, CD8⁺ T cells were enriched from spleens and purified as $CD8\alpha^+Thy1.1^+CD44^+CD62L^+$ T_{CM} cells by flow cytometric sorting. Sorted cells were co-cultured with naïve splenocytes and stimulated with SIINFEKL peptide for 4 h in the presence of brefeldin A and anti-CD107a to assess cytokine production and degranulation. Cells were subsequently processed for intracellular staining according to standard protocols. **(E)** Representative flow cytometry plots gated on OTI CD8 T cells. **(F)** Frequencies of $CD107a^+$, $GzmA^+$, $IFN\gamma^+$, and $TNF\alpha^+$ among the OTI $CD8^+$ T cell population were quantified. $N = 4$ per group, representative of two dependent experiments. Multiple Mann–Whitney tests were used for statistical comparisons, with significance denoted as *P < 0.05 and "ns" indicating not significant. Error bars represent mean ± SEM.

resident DCs (cDCs, $CD11c^+$ $MHCII^{med}$) from migratory DCs (migDCs, $CD11c^+$ $MHCII^{high}$) by MHCII expression levels (Fig. S4 A). Results showed a significant reduction in the frequency of migDCs in the dLNs of nociceptor-deficient mice compared with nociceptor-sufficient mice (Fig. 5 A). The total number of migDCs was also lower in *Trpv1-DTA* mice, whereas cDC numbers remained unchanged. We further analyzed subpopulations of migDCs based on markers such as CD326, CD103, CD207 (Langerin), XCR1, CD11b, and CD24. Migrated LC subsets ($CD326^+$ $CD103^{lo}$, migLCs) were markedly reduced in the dLNs of *Trpv1-DTA* mice in terms of both frequency and number (Fig. 5 B). However, other migDC subsets showed minimal or no differences compared with controls (Fig. S4, B and C). Consistent with neuron-ablated mice, mice lacking the CGRP receptor Ramp1 ($Ramp1^{-/-}$ mice) also exhibited significantly lower migLCs in the dLNs compared with $Ramp1^{+/+}$ mice (Fig. S4, D and E).

To further investigate the role of sensory neurons in LC antiviral responses, we infected mice with VACV-GFP virus and analyzed viral uptake by immune cells using flow cytometry. The results showed that most GFP⁺ cells in the dLNs are migratory LC cells, with a significantly lower percentage of GFP⁺ and migLCs detected in neuron-ablated mice compared with *DTA* control mice (Fig. 5, C and D). Given these observations, as

Downloaded from rupress.org/jem/article-pdf/223/12/e20261215/2044247/jem_20261215.pdf by University of California Irvine user on 16 November 2026

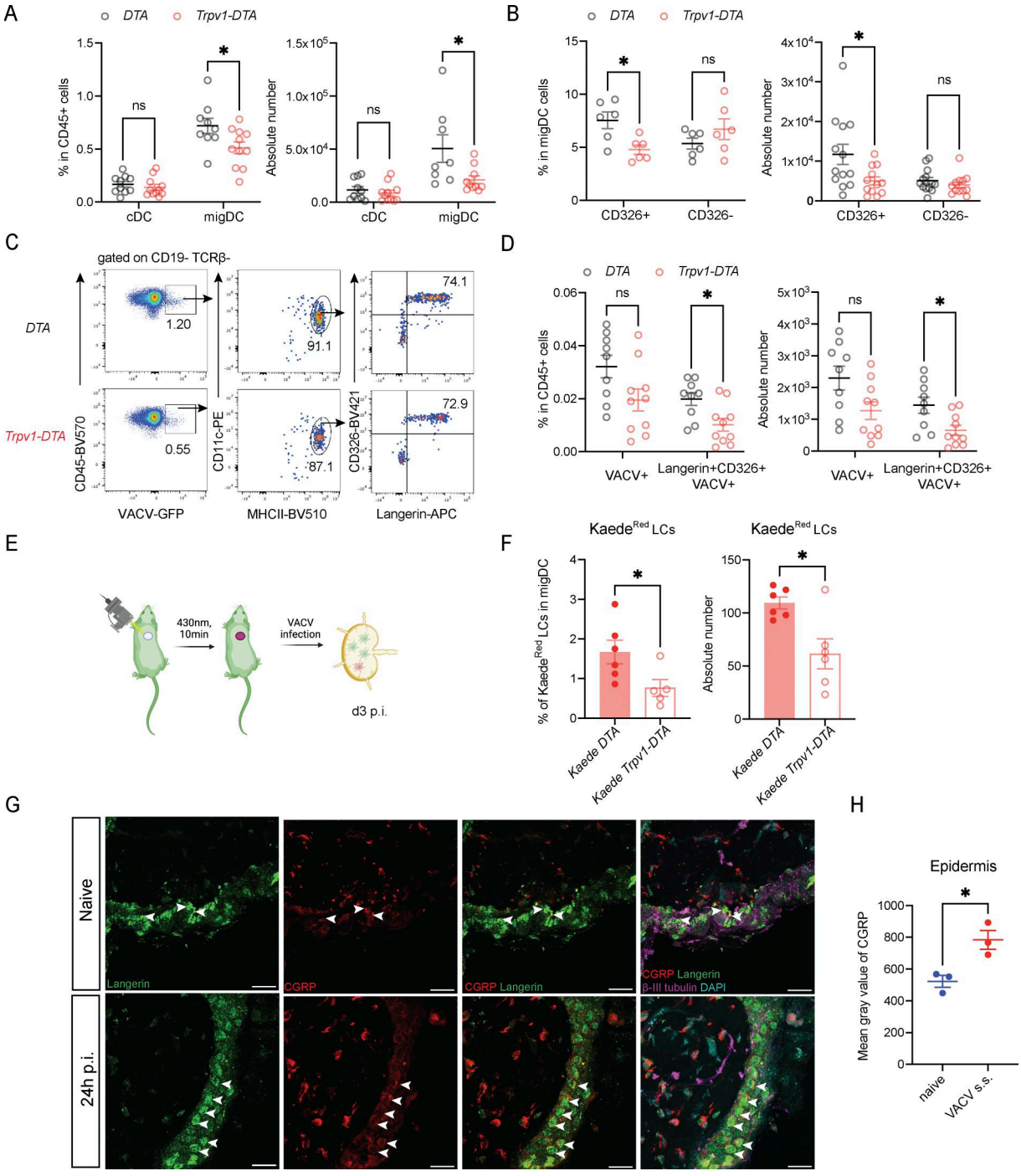

Figure 5. **VACV s.s.-induced migration of LCs into dLNs requires Trpv1⁺ sensory neurons. (A)** Percentages and numbers of resident conventional DCs (cDCs) and migDCs in dLNs of *DTA* and *Trpv1-DTA* mice 72 h after VACV immunization via s.s. *N* = 8–10 mice per group pooled from two independent experiments. **(B)** Percentages and absolute numbers of two migDC subsets: Langerin⁺CD103⁻CD326⁺ (CD326⁺) and Langerin⁺CD103⁺CD326⁻ (CD326⁻) in dLNs as analyzed in A. **(C)** Flow cytometry gating of VACV-GFP–positive cells between DTA and Trpv1-DTA mice. **(D)** Percentages and absolute numbers of VACV⁺ and VACV⁺Langerin⁺CD326⁺ cells in the dLNs of mice 72 h after VACV-GFP s.s. *N* = 9–10 mice per group pooled from two independent experiments. **(E)** Experimental setup of *Kaede x DTA* or *Kaede x Trpv1-DTA* mice. 72 h after photoconversion and VACV immunization, dLNs were collected for flow cytometry analysis. **(F)** Percentages and total numbers of live Kaede^red Langerin⁺CD326⁺ DCs in dLNs, as indicated in E. *N* = 5–6 mice per group, representative of two independent experiments. **(G)** Representative images of CGRP (red) and Langerin (green) expression in skin from naive mice or mice treated with VACV via s.s. Images were acquired 24 h after treatment. Scale bars, 20 µm. **(H)** Mean gray value of CGRP in the epidermal region between naïve and virus-infected group with each data point used representing a single mouse. *N* = 3 mice per group from one experiment. Mann–Whitney test (F), Multiple Mann–Whitney test (A, B, and D), and unpaired *t* test (H) were used for statistical comparisons, with significance denoted as *P < 0.05, and "ns" indicating not significant. Error bars represent mean ± SEM. **(E)** Figure adapted from an image created in BioRender.

Downloaded from rupress.org/jem/article-pdf/223/12/e20261215/2044247/jem_20261215.pdf by University of California Irvine user on 16 November 2026

well as the known interplay between sensory neurons and DCs, we hypothesized that sensory neurons activated by skin VACV s.s. infection may signal to LCs to promote their migration to the dLNs.

To directly assess LC migration following VACV s.s., we used Kaede mice that express a photoconverted protein that transitions from green to red fluorescence upon exposure to violet light, which allows the tracking of cells originating from the site of photoconversion and antigen exposure (Kaede^{Red}) (Park et al., 2018). We generated *Kaede x Trpv1-DTA* and *Kaede x DTA* mice. Mice were first photoconverted on the skin for 10 min and then infected with VACV via s.s. dLNs were collected 3 days after infection for flow cytometry analysis (Fig. 5 E). Our analysis revealed significantly fewer Kaede^{Red} LCs in dLNs of *Kaede x Trpv1-DTA* mice compared with *Kaede x DTA* mice, both in terms of percentages and cell numbers (Fig. 5 F). We also observed a similar decrease in migratory LCs in *Kaede x Ramp1*$^{-/-}$ compared with *Kaede x Ramp1*$^{+/+}$ following photoconversion (Fig. S4 F).

To further assess the spatial relationship between CGRP$^+$ sensory fibers and LCs in the skin, we performed immunofluorescence staining for CGRP and Langerin in epidermal sections. In naïve skin, CGRP$^+$ nerve fibers were readily detected within the epidermis and frequently localized in close proximity to LCs, positioning LCs to sense neuron-derived neuropeptides under steady-state conditions (Fig. 5, G and H). Following VACV immunization via s.s., CGRP immunoreactivity within the epidermis was significantly increased compared with naïve controls (Fig. 5, G and H). This increase was accompanied by an apparent enrichment of CGRP signal in regions adjacent to LC$^+$, consistent with enhanced local availability of CGRP in the epidermal LC niche during infection.

In addition to migration analysis, we also measured the expression levels of three co-stimulatory molecules (CD40, CD80, and CD86) that are critical for antigen presentation (Cabeza-Cabrerizo et al., 2021). Although prior studies have reported that CGRP can inhibit the antigen-presenting capacity of LCs under certain inflammatory or pathological conditions (Hosoi et al., 1993a), we did not observe significant changes in the surface expression of these co-stimulatory molecules on LCs in the absence of nociceptor neurons or Ramp1 (Fig. S4, G and H). These differences likely reflect the context-dependent nature of CGRP signaling, which can exert distinct effects on immune cells depending on the inflammatory milieu, duration of exposure, and disease setting. These results collectively highlight the critical role of the CGRP-Ramp1 axis and sensory neurons in facilitating the migration of LCs to the dLNs, which is associated with enhanced CD8$^+$ T cell responses following VACV immunization.

Deficiency of Ramp1 signaling in OT-I T cells does not alter the memory CD8 T cell response

Given that T cells have been reported to express the CGRP receptors, including Ramp1, which can mediate their differentiation and function (Kulalert et al., 2024; Zhu et al., 2024; Hou et al., 2024), we sought to determine whether CGRP could act directly on OT-I T cells through Ramp1. To address this, we crossed *Ramp1*$^{-/-}$ mice to *OT-I/Rag1*$^{-/-}$*/Thy1.1*$^{+/+}$ mice to generate Ramp1-deficient OT-I T cells. *Ramp1*$^{+/+}$ or *Ramp1*$^{-/-}$ OT-I T cells were then adoptively transferred into host mice, which were subsequently infected with VACV-OVA via s.s. as described previously (Fig. S4 I). Flow cytometry analysis on skin and LN revealed no significant decrease in the percentages or numbers of OT-I T cells between the two groups in the memory phase (Fig. S4, J and K). However, there was a slight increase in OT-I T cell numbers in the dLN (Fig. S4 K). These results indicate that the promotive effect of CGRP-RAMP1 signaling on the T cell memory response is not mediated directly through T cells.

LCs are required for CGRP-Ramp1–mediated enhancement of memory CD8 T cell responses

We next determined the role of LCs in response to VACV inoculated by s.s. in transgenic mice expressing the DT receptor under the control of the murine Langerin promoter (*Lang-DTR*) mouse model (Kissenpfennig et al., 2005). With i.p. injection of DT, all LC$^+$ will be depleted, including LCs and dermal Langerin$^+$ DCs (Langerin$^+$ dDCs). However, LC repopulation is delayed for several weeks, whereas Langerin+ dDCs are replenished within a few days (Bursch et al., 2007).

To distinguish the effects of distinct LC$^+$ populations during VACV exposure, *Lang-DTR* mice were treated systemically with DT using two different schedules. Mice receiving DT 13 days prior to immunization were used to selectively deplete epidermal LCs (LC-depleted group), whereas mice receiving DT both 13 days and 1 day prior to immunization were used to deplete both LCs and Langerin$^+$ dDCs (Langerin$^+$ DC–depleted group). To validate this model, we quantified epidermal LCs and Langerin$^+$ dDCs in naïve skin following DT administration. Langerin$^+$ dDC numbers in the LC-depleted group had recovered to levels comparable with those in control mice, whereas LCs remained markedly reduced (Fig. S5, A and B). In contrast, when mice received DT injections at both day −13 and day −1, both epidermal LCs and Langerin$^+$ dDCs were undetectable (Fig. S5, A and B). These data support the use of this approach to selectively assess the contribution of LCs in our experimental context. We next assessed these populations in the dLNs following immunization. After a single injection of DT 13 days before immunization, no LCs can be detected in the dLNs 3 days p.i., and Langerin$^+$ dDCs returned compared with non-treated vehicle group (Fig. S5, C–E). However, all the Langerin$^+$ dDCs are completely absent when DT is injected 13 days and 1 day before immunization (Fig. S5, C–E).

Taking advantage of this mouse model, we selectively depleted LCs alone by injecting DT systemically 13 days before immunization. Following LC depletion, we adoptively transferred OT-I T cells and infected the mice with VACV-OVA via s.s. the next day (Fig. 6 A). Flow cytometry analysis revealed a significant reduction in CD8$^+$ OT-I T cells in the absence of LCs at 28 days p.i. (Fig. 6 B). In a separate experiment, Lang-DTR mice were infected with VACV-OVA s.c., and LCs were either depleted by DT treatment or left intact. Mice were then administered PBS or CGRPα daily for the first 6 days p.i., followed by administration every other day until day 28 after infection (Fig. 6 C). dLNs were subsequently harvested and analyzed by flow cytometry. No significant differences in either the number or frequency of

Downloaded from rupress.org/jem/article-pdf/223/12/e20261215/2044247/jem_20261215.pdf by University of California Irvine user on 16 November 2026

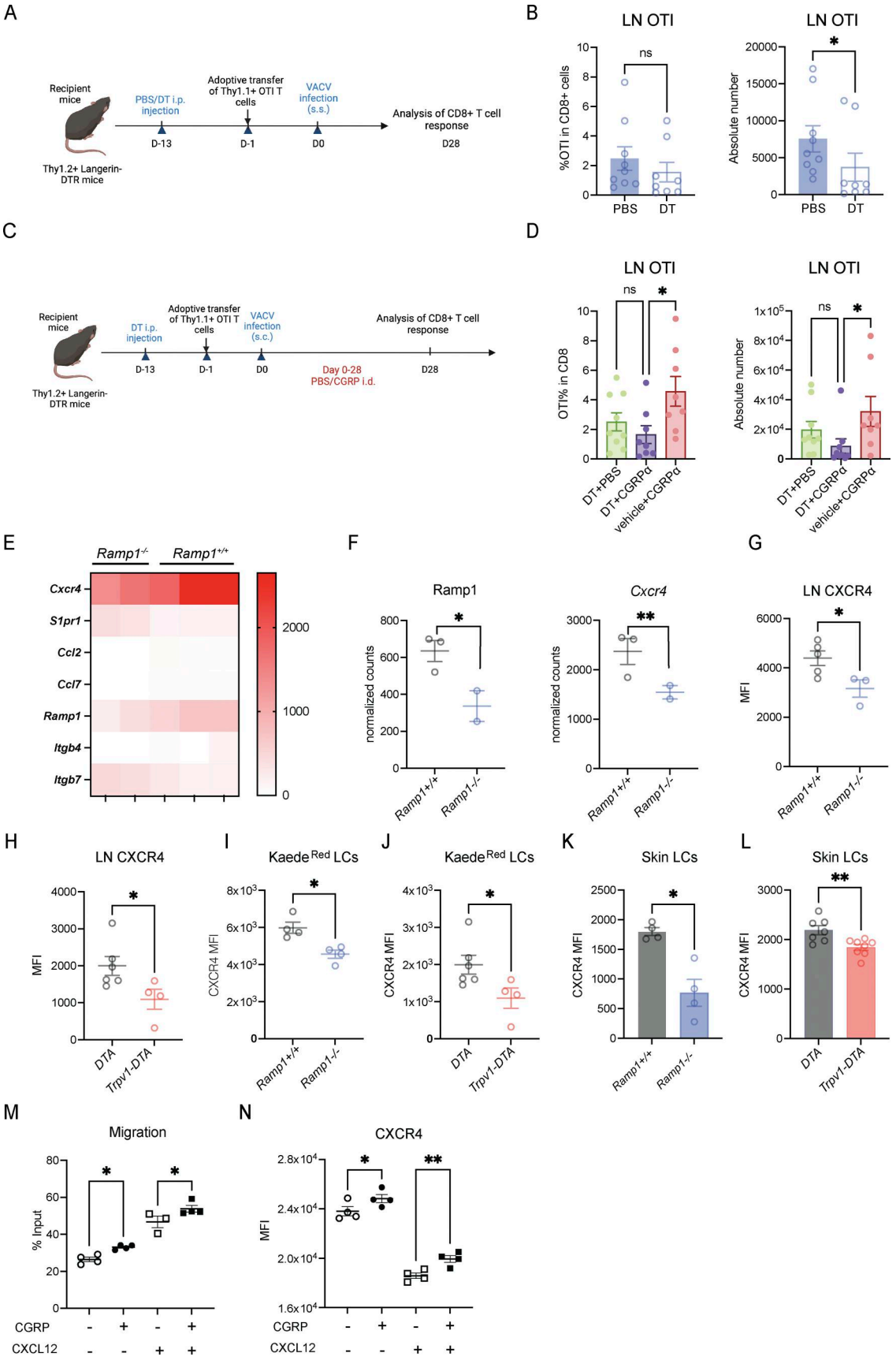

Figure 6. **Regulation of LC migration by CGRP-Ramp1 signaling is required for induction of the antiviral CD8 T cell response. (A)** Experimental design to determine the effect of skin LCs on CD8⁺ T cell response during VACV s.s. Mice were injected with PBS/DT i.p. 13 days before infection. OT-I T cells were

Downloaded from rupress.org/jem/article-pdf/223/12/e20261215/2044247/jem_20261215.pdf by University of California Irvine user on 16 November 2026

determined through flow cytometry 28 days after infection. **(B)** Percentages and absolute numbers of virus-specific CD8 T cells (Thy1.1$^+$ OT-I) in the LN were determined on day 28 after infection in both PBS-treated and DT-treated groups. *N* = 8–9 mice per group, pooled from two independent experiments. **(C)** Experimental design to determine the effect of CGRP-Ramp1 signaling on CD8$^+$ T cell response during VACV s.s. Mice were injected with DT i.p. 13 days before VACV-OVA immunization s.c. and treated daily for the first 6 days p.i., followed by treatment every other day until day 28. OT-I T cells were determined through flow cytometry 28 days after infection. **(D)** Percentages and absolute numbers of virus-specific CD8 T cells (Thy1.1$^+$ OT-I) in the dLNs were determined on day 28 after infection in the PBS-treated and CGRPα-treated groups. *N* = 5 mice per group, representative of two independent experiments. **(E)** Representative heatmap showing significantly differentially expressed migration-associated genes (p value <0.05) from bulk RNA-seq of migrating LCs from dLNs of *Ramp1*$^{+/+}$ and *Ramp1*$^{-/-}$ immunized mice. **(F)** *Ramp1* and *Cxcr4*-normalized counts in Langerin$^+$CD326$^+$ migrating LCs from dLNs of *Ramp1*$^{+/+}$ and *Ramp*$^{-/-}$ mice. **(G and H)** CXCR4 expression level in Langerin$^+$CD326$^+$ migrating LCs from dLNs of G *Ramp1*$^{+/+}$ and *Ramp*$^{-/-}$ mice or H *DTA* and *Trpv1-DTA* mice from flow cytometry analysis. *N* = 3–6 mice per group, representative of two independent experiments. **(I and J)** *Kaede* mice from specific genotypes were photoconverted and VACV immunized. 72 h later, dLNs were collected for flow cytometry analysis. CXCR4 expression in Kaede^{red}-migrating LCs of LNs from either (I) *Ramp1*$^{-/-}$ and *Ramp1*$^{+/+}$ mice or (J) *Trpv1-DTA* and *DTA* mice at 3 days p.i. Data in I are from *n* = 4 mice per group representative of two independent experiments; data in J are from *n* = 4–6 mice per group pooled from two independent experiments. **(K and L)** LCs in the epidermis were analyzed by flow cytometry for CXCR4 expression at 3 days p.i. from (K) *Ramp1*$^{-/-}$ and *Ramp1*$^{+/+}$ and (L) *Trpv1-DTA* and *DTA* mice. Data in K are from *n* = 4 mice per group from one experiment; data in L are from *n* = 7–8 mice per group pooled from two independent experiments. **(M)** Epidermal cell suspensions (1×10^6) were applied to the upper chamber of transwell. 50 nM CXCL12 and/or 1 nM CGRPα were administered to the lower chamber. Migrated epidermal LCs were identified as MHC II$^+$ subsets in the lower chamber. The % input was calculated as follows: (the number of LCs migrated into the lower chamber)/(the number of LCs applied into the upper chamber) × 100. *N* = 3–4 per group, representative of two independent experiments. **(N)** CXCR4 expression level of migrated LCs treated as indicated in I from cytometry analysis. *N* = 4 per group, representative of two independent experiments. Mann–Whitney test (B, D, G, and H) and multiple Mann–Whitney test (M and N) were used for statistical comparisons, with significance denoted as *P < 0.05, **P < 0.01, and "ns" indicating not significant. Error bars represent mean ± SEM. **(A and C)** Figures adapted from images created in BioRender.

OT-I T cells were observed between PBS- and CGRPα-treated groups in DT-treated Lang-DTR mice (Fig. 6 D). In contrast, in control Lang-DTR mice that did not receive DT, CGRPα treatment markedly increased OT-I cell numbers in the dLNs compared with DT-treated mice receiving CGRPα (Fig. 6 D). Taken together with previous findings, these results suggest that LCs are an important cellular target of CGRP/Ramp1 signaling during the generation of memory T cell responses.

To investigate the molecular mechanisms underlying CGRP-Ramp1 signaling in LCs, we purified migrated LCs from dLNs of *Ramp1*$^{+/+}$ and *Ramp1*$^{-/-}$ mice 3 days p.i. with VACV and performed RNA-sequencing (RNA-seq) analysis (Fig. S5, F and G; and Table S1). The number of biological replicates was constrained by technical limitations, as isolation of sufficient numbers of Langerin$^+$CD326$^+$ DCs for bulk RNA-seq required pooling dLNs from three to five mice per sample. Despite this limitation, differential expression analysis was conducted in DESeq2 (version 1.46.0) with standard normalization and dispersion estimation. Our previous results revealed that LC migration is significantly impaired in the absence of CGRP-Ramp1 signaling (Fig. 5). Given this observation, we focused on the genes associated with LC migration (Fig. 6 E and Table S1). It has been reported that LC migration to skin dLNs occurs in two distinct phases: a first step from the epidermis to the dermis regulated by CXCR4 during the early stages of migration, followed by CCR7-mediated migration to the dLNs (Redpath et al., 2017; Kabashima et al., 2007). RNA-seq analysis of migrating LCs demonstrated a significant reduction in Ramp1 expression in Ramp1-deficient LCs (P <0.01). Interestingly, we observed a marked decrease in *Cxcr4* mRNA level in *Ramp1*$^{-/-}$ migrating LCs (Fig. 6, E and F). To confirm this finding, we assessed CXCR4 protein levels by flow cytometry in control and *Ramp1*$^{-/-}$ LCs following VACV infection. The reduction in CXCR4 expression was consistent at both the protein and mRNA levels (Fig. 6 G). Additionally, in nociceptor-ablated mice (*Trpv1-DTA*), the migrated LCs in the dLN exhibited lower CXCR4 expression compared with control *DTA* mice (Fig. 6 H). In contrast, CCR7 expression was unchanged at both the mRNA and protein levels in *Ramp1*$^{-/-}$ and control LCs and Langerin$^+$ dDCs (Fig. S5, H–K). To specifically determine whether the migrating cells in the dLNs were derived from epidermal LCs, we used Kaede photoconvertible mice to fate-map skin-resident LCs migrating to the dLNs. We analyzed CXCR4 expression on Kaede-labeled migrating LCs and found that CXCR4 expression was significantly reduced in Ramp1-deficient migrating LCs compared with controls (Fig. 6 I). A similar reduction was observed in *Trpv1-DTA* mice relative to *DTA* controls (Fig. 6 J). In addition, to address whether CXCR4 expression is altered in skin-resident LCs, we assessed CXCR4 levels in LCs isolated directly from the skin and found that CXCR4 expression was reduced in LCs isolated from the epidermis in the absence of Ramp1 (*Ramp1*$^{-/-}$ mice) or nociceptor neurons (*Trpv1-DTA* mice) 3 days after infection (Fig. 6, K and L), whereas no significant differences were observed in the skin at steady-state conditions (Fig. S5, L and M). These data demonstrate that the observed reduction in CXCR4 expression is specific to LCs that migrated from the skin, rather than reflecting changes in other migDC subsets.

To further validate the role of CGRP-Ramp1 signaling in promoting LC migration via CXCR4 upregulation, we assessed the chemotactic response of LCs to CXCR4 ligand (CXCL12) and CGRP agonist using a transwell migration assay. Epidermal cell suspensions were placed in the upper chamber, while the lower chamber contained CXCL12, CGRP, or both. The migrated epidermal LCs were identified as MHC class II+ cells in the lower chamber. The addition of CGRP to the lower chamber enhanced LC chemotaxis both in the presence and absence of CXCL12 (Fig. 6 M). Furthermore, CGRP stimulation significantly upregulated CXCR4 expression in LCs (Fig. 6 N). A reduction in CXCR4 levels was observed in LCs following CXCL12 treatment (Fig. 6 N), likely due to ligand-induced internalization (Cole et al., 1999). However, no upregulation was observed in terms of CCR7 expression upon stimulation with CGRP (Fig. S5 N). Collectively, integrating results from in vivo Kaede photoconversion, nociceptor ablation models, and genetic disruption

Downloaded from rupress.org/jem/article-pdf/223/12/e20261215/2044247/jem_20261215.pdf by University of California Irvine user on 16 November 2026

of RAMP1 signaling, these findings suggest that CGRP-Ramp1 signaling facilitates LC migration from the epidermis to the dermis in the context of VACV infection through the regulation of CXCR4 in LCs.

Discussion

The role of pain signaling in modulating the vaccine-induced adaptive immune response has not been extensively studied. Although sensory neurons have been implicated in antiviral CD8⁺ T cell responses, how nociceptor-derived signals influence the development of long-term T cell memory following cutaneous vaccination remains unclear. Here, we established that VACV infection via s.s. induces nociceptor neuron activation and robust release of neuropeptide CGRP in the skin. CGRP-Ramp1 signaling promotes migration of skin LCs from the epidermis to the dermis and dLNs in the end. In addition, the nociceptor-CGRP-Ramp1 signaling axis provides protection during VACV-WR rechallenge p.i. CGRP intradermal treatment can promote the memory T cell response 4 wk after the first infection. Our findings reveal a role for nociceptor neurons in promoting memory T cell response and highlight the potential of leveraging the CGRP-Ramp1-LCs axis in vaccine development.

Sensory neurons are increasingly recognized as important regulators of adaptive immune responses in the skin. Filtjens et al. demonstrated that sensory neurons are required for robust CD8⁺ T cell priming in skin dLNs during HSV-1 infection by regulating DC responses, establishing an important role for nociceptors in antiviral adaptive immunity (Filtjens et al., 2021). However, the molecular signals linking sensory neuron activation to APC function and whether this neuroimmune interaction influences the establishment of long-term T cell memory remained unclear. More recently, Huang et al. showed that CGRP can directly regulate RAMP1-expressing CD8⁺ T cells in Stevens–Johnson syndrome/toxic epidermal necrolysis, demonstrating that CGRP-RAMP1 signaling can modulate effector T cell function in inflammatory skin disease (Huang et al., 2025). Interestingly, we did not observe a difference in the responses of adoptively transferred WT and *Ramp1*$^{-/-}$ OT-I cells following VACV s.s., suggesting that T cell–intrinsic RAMP1 signaling is not required for the memory CD8⁺ T cell response in our model. Instead, our study extends these findings by defining a distinct neuroimmune circuit in the context of cutaneous vaccination, in which CGRP-RAMP1 signaling links nociceptor activation to LC trafficking and, ultimately, the establishment of protective CD8⁺ T cell memory. These findings suggest that the cellular targets and immunological consequences of CGRP-RAMP1 signaling are context-dependent: whereas CGRP can act directly on effector CD8⁺ T cells in inflammatory skin disease, during cutaneous VACV vaccination, its effects on CD8⁺ T cell immunity appear to be mediated predominantly through regulation of APCs. These findings expand the role of sensory neurons from the regulation of primary or effector CD8⁺ T cell responses to the generation of long-term adaptive immune memory.

By using skin explants from infected mice, we detected a large amount of CGRP release into the skin following VACV s.s., while no difference was detected in SP levels. This is interesting as SP has also been shown to drive DC responses and promote downstream allergic immunity. Although CGRP and SP are frequently co-expressed in nociceptor neurons, SP levels in our skin explant assays were near the limit of detection, precluding reliable quantification of changes following VACV infection. Thus, while a contribution of SP cannot be excluded, our study focuses on CGRP, which was consistently detectable following s.s. and functionally linked to downstream immune responses in this context. By contrast, CGRP release was not induced by intradermal or s.c. inoculation. While VV s.c. did not elicit detectable CGRP release, this does not preclude contributions from other nociceptors, including CGRP-independent signaling pathways or non-peptidergic neuronal populations. It is possible that this is a result of the concentration of peptidergic nociceptor innervation of the epidermal/dermal junction and also suggests a role for CGRP-expressing nociceptors in smallpox vaccine efficacy. Nociceptor sensory neurons are tasked with protecting the organism from threats by initiating the sensation of pain and eliciting defensive behaviors. We found that pain was strongly induced as early as 2 h after infection, while RTX-treated mice, lacking functional CGRP-expressing nerves, did not exhibit pain upon s.s. in the early phase. Interestingly, a second peak in pain onset occurred at day 5 after infection, coinciding with a second CGRP peak, which is most likely associated with the VACV-induced inflammatory milieu. Heat pain modulatory was completely eliminated in RTX-treated mice at all examined time points, whereas mechanical hypersensitivity was suppressed during the early phase but reappeared at day 5. These findings suggest Trpv1⁺ neurons mediate multiple pain modalities, including all of the heat pain and the early phase of mechanical pain sensitivity, while later mechanical pain may involve additional sensory neuron subsets (Kupari and Ernfors, 2023).

The peripheral nervous system is one of the earliest responders to skin injuries. Upon injury, nociceptor neurons transduce action potentials to the central nervous system to trigger pain perception. Simultaneously, antidromic signaling and calcium influx in sensory nerve endings lead to the local release of neuropeptides in tissues (Gouin et al., 2017; Cañedo-Dorantes and Cañedo-Ayala, 2019). Nociceptors are sensitized by immune mediators such as cytokines as well as pathogen-derived molecules such as bacterial toxins, lipopolysaccharides, and flagellin (Baral et al., 2019). Whether the VACV or its molecular products directly activate nociceptor neurons, or if pain is driven primarily by the injury or immune response during the scarification process, remains to be clarified.

We next found that CGRP/Ramp1 signaling mediated the memory CD8⁺ T cell response by impacting both the numbers and activation of OT-I cells in the dLNs. By contrast, we observed no obvious difference in skin antigen-specific T cell counts between infected nociceptor-deficient and -sufficient mice, suggesting that skin memory T cells may be less dependent on nociceptor-derived signals. Notably, however, direct pharmacological manipulation of CGRP signaling with CGRPα or CGRP8-37 affected the skin memory CD8⁺ T cell compartment, indicating that neuronal depletion and sustained manipulation of CGRP-RAMP1 signaling are not fully equivalent. One possible explanation is that CGRPα and CGRP8-37 were administered

Downloaded from rupress.org/jem/article-pdf/223/12/e20261215/2044247/jem_20261215.pdf by University of California Irvine user on 16 November 2026

repeatedly throughout the development of the memory response and therefore may not recapitulate the physiological magnitude and temporal dynamics of sensory neuron-derived CGRP release. Our current experiments do not distinguish among these possibilities, and therefore the contribution of the TRPV1$^+$ sensory neuron-CGRP axis to the skin-resident memory compartment appears to be more complex than its effect in the dLNs.

Previous studies have demonstrated that CD8$^+$ T cells that have entered peripheral tissues such as skin can become locally retained and persist independently of continued input from the circulation or the dLN pool (Mackay et al., 2012). In this context, Trpv1$^+$ nociceptor ablation selectively impairs LC migration to the dLN, potentially limiting antigen delivery and/or T cell activation within the dLNs, leading to reduced OT-I cell numbers. Once effector T cells seed the skin, their local maintenance and persistence are largely uncoupled from LN dynamics, allowing skin OT-I numbers to remain unchanged despite reduced LN accumulation. Furthermore, we found CGRP-Ramp1 signaling is important in protecting the mice from cutaneous VACV-WR challenge, with lower viral gene expression at the inoculation site. While exogenous CGRP administration provides a functional tool to probe CGRP-dependent effects, future studies using optogenetic or chemogenetic manipulation of Trpv1-expressing sensory neurons will be valuable for more faithfully recapitulating physiological functions of peptide release.

CD8$^+$ memory T cells are classified as a population that can persist in the long term and respond quickly upon reactivation. They have been broadly subdivided into three subpopulations: central memory, effector memory, and T_{RM} cells. T cell–dependent control of viral infection can start with T_{RM} providing defense against secondary infection at the frontline, which can be further reinforced with recruitment of T_{EM} from the circulation and expansion of T_{CM} cells in the dLNs to ensure complete control and elimination of an invading pathogen (Wherry et al., 2003; Kohlmeier and Woodland, 2009). Although we did not observe changes in the T_{RM} population in the absence of CGRP-Ramp1 signaling, we found a significant reduction in memory T cell numbers in the LNs. We propose that skin-resident T_{RM} may act as local alarm cells (Rotrosen and Kupper, 2023) due to their strategic positioning within peripheral tissues. Upon antigen re-encounter, these cells may contribute to the initiation of recall immune responses, which could facilitate the participation of both T_{EM} and T_{CM} in dLNs, thereby enhancing protection against reinfection and accelerating pathogen clearance. At the same time, we acknowledge that CD4$^+$ T cells play essential roles in skin immunity, including regulation of inflammation and coordination of antiviral responses, as highlighted by recent studies (Harbour et al., 2023; Liu et al., 2010). The present work does not aim to comprehensively dissect CD4$^+$ T cell contributions, but rather focuses on defining how nociceptor signaling shapes CD8$^+$ T cell memory within this broader immune context. How nociceptor–immune interactions influence CD4$^+$ T cell responses represents an important direction for future investigation.

LCs are the only epidermis-resident APCs that share a common ontogeny with macrophages but function as DCs. CGRP-expressing nerve fibers are physically associated with LC dendrites in human epidermis, and CGRP is found at the surface of some LCs by confocal laser microscopy (Hosoi et al., 1993b). Using CGRP immunostaining, we observed CGRP$^+$ nerve fibers within the epidermis in close proximity to LCs (Langerin$^+$ in epidermis), consistent with the idea that LCs are positioned to sense neuropeptides locally. Importantly, following VACV s.s., we detected an increase in CGRP signal within the epidermis and enhanced apparent association with LCs, suggesting that infection-induced nociceptor activation increases local CGRP availability in the epidermal microenvironment.

Our study revealed that CGRP-Ramp1 signaling promotes LC migration to the dLN. Fewer migrating LCs were detected in the dLNs of *Ramp1*$^{-/-}$ and *Trpv1-DTA* mice 3 days after infection. Using Kaede photoconvertible mice, we further demonstrated that this defect reflects impaired trafficking of skin-resident LCs from the epidermis to the dLNs during viral infection. In the absence of nociceptor signaling, this migratory defect is associated with reduced CXCR4 expression on Cs and likely contributes to the observed defects in downstream T cell responses. However, because Ramp1 deficiency in our experiments is germline rather than restricted to LCs, these findings do not formally establish that RAMP1 functions intrinsically within LCs. We therefore cannot exclude the possibility that CGRP acts through RAMP1 on another CGRP-responsive cell population that subsequently influences LC migration or function. LC-specific deletion of Ramp1, or complementary cell-transfer approaches, will be required to distinguish a direct LC-intrinsic role for RAMP1 from indirect regulation through other cell populations.

Whereas CGRP has been reported to inhibit dermal DC migration through CCR7 downregulation in contact hypersensitivity models (Mikami et al., 2011), we find that CGRP enhances LC migration in the setting of viral infection by modulating CXCR4 expression rather than CCR7. These opposing effects highlight the context-dependent nature of CGRP-RAMP1 signaling, which differentially regulates DC migratory programs depending on DC subset identity and the surrounding inflammatory milieu. Dynamic intravital imaging has shown that VACV peptides can be presented to prime MHCI-restricted CD8$^+$ T cells through either direct or cross-presentation (Xu et al., 2010; Heipertz et al., 2014). Although CGRP signaling promotes LC migration to the dLNs, multiple DC subsets are likely to contribute to naïve CD8$^+$ T cell priming. While migratory LCs may transport antigen and modulate the local immune milieu, CD103$^+$ dermal DCs, CD301b$^+$ dermal DCs, and LN-resident CD8α$^+$ cDC1s are well established as key cross-presenting populations (Kashem et al., 2017; Henri et al., 2010; Allan et al., 2003; Tamoutounour et al., 2013; Kissenpfennig et al., 2005; Perner et al., 2020). Our findings therefore support a model in which CGRP-dependent LC migration shapes antigen availability and priming efficiency within the dLNs, rather than directly defining the identity of the dominant APC. Further studies using subset-specific models, such as XCR1-DTR mice, will be necessary to precisely define how nociceptor signaling modulates distinct DC subsets and their respective roles in shaping antiviral immunity.

CGRP is also a well-established vasodilator (Brain et al., 1985), and its effects on the local microvasculature could, in principle,

Downloaded from rupress.org/jem/article-pdf/223/12/e20261215/2044247/jem_20261215.pdf by University of California Irvine user on 16 November 2026

influence immune cell trafficking within inflamed skin. However, whether CGRP-mediated vasodilation directly contributes to LC migration during viral infection remains to be determined. While our data provide strong functional evidence for the CGRP-RAMP1 axis in programming LC migration, the detailed molecular mechanisms connecting this signal to CXCR4 regulation were not addressed in the current study. Based on established literature in other immune cells (Russell et al., 2014), we speculate that downstream activation of the cAMP-PKA pathway and transcription factors like CREB may be involved. A direct investigation of these signaling intermediates in LCs represents a critical avenue for future research.

Pain is a defining feature of many diseases and has been shown to play a pivotal role in modulating immune responses (Baral et al., 2019). Notably, s.s. as an immunization route induces pain, which enhances the CD8$^+$ T cell memory responses through the CGRP/Ramp1/LCs axis. Furthermore, early pain deprivation significantly impairs the CD8$^+$ T cell immune response. These findings highlight the critical role of neuroimmune cross talk, offering promising new avenues for the development of next-generation vaccines.

Materials and methods

Mice

WT *C57BL/6J* (RRID:IMSR_JAX:000664), B6.PL-*Thy1a*/CyJ (*Thy1.1*$^{+/+}$, RRID:IMSR_JAX:000406), *B6.129S7-Rag1tm1Mom/J* (*Rag1*$^{-/-}$, RRID:IMSR_JAX:002216), *C57BL/6-Tg(TcraTcrb)1100Mjb/J* (*OT-I*, RRID:IMSR_JAX:003831), *B6.129S2(Cg)*-Ramp1tm1.1Tsuj/WkinJ (*Ramp1*$^{-/-}$, *RRID:IMSR_JAX:031560*), *Trpv1-Cre*$^{+/+}$ *B6.129-Trpv1tm1(cre)Bbm/J* (*Trpv1-Cre*, RRID:IMSR_JAX:017769), *B6.Rosa26-stop(flox)-DTA* (*Rosa-DTA*, RRID:IMSR_JAX:009669), and *B6.129S2-Cd207tm3.1(HBEGF/EGFP)Mal/J* (*Cd207-DTR/EGFP*, RRID:IMSR_JAX:016940) mice were purchased from The Jackson Laboratory. *OT-I/Rag1*$^{-/-}$*/Thy1.1*$^+$ mice were maintained through routine breeding in the animal facility of the Harvard Institute of Medicine, Harvard Medical School. *Trpv1-Cre*$^{+/-}$ mice were crossed with Rosa26-stop(flox)-DTA$^{+/+}$ to generate Trpv1-lineage neuron-depleted *Trpv1-Cre*$^{+/-}$*; DTA*$^{+/-}$ (*Trpv1-DTA*) mice and control *Trpv1-Cre*$^{-/-}$*; DTA*$^{+/-}$ (*DTA* Ctrl) littermates. *Kaede* mice were originally from Osami Kanagawa (Brain Science Institute, Riken, Hirosawa, Japan) and were crossed with *Trpv1-DTA* mice to generate *Kaede x Trpv1-DTA* mice.

Both male and female mice were used in this study. Experimental and control groups were sex-matched within each experiment. Mice were randomly allocated to experimental groups before the initiation of each experiment. Animal experiments were performed in accordance with the guidelines implemented by the Center for Animal Resources and Comparative Medicine of Brigham and Women's Hospital or Harvard Medical School. Mice were bred and maintained in a specific pathogen–free animal facility at Brigham and Women's Hospital.

Virus and infections

Recombinant VACV expressing the OT-I T cell epitope $OVA_{257-264}$ (VACV-OVA) and Western Reserve strain (VACV-WR) were originally obtained from B. Moss (National Institutes of Health, Bethesda, MD, USA). The virus was expanded and titrated by standard procedures as described previously (Liu et al., 2010). 2×10^6 pfu of VACV-OVA was used for infection by s.s., intradermal, or s.c. infection. For s.s. infection, mice were anesthetized, and the dorsal skin was shaved and cleaned. 10 µl of diluted virus was applied to the skin and was then gently scratched 25 times with a 28 1/2-G needle. 2×10^6 pfu VACV-WR was used for skin challenge after first immunization, as described previously (Liu et al., 2010). For behavioral assays only, s.s. was performed on the hindpaw rather than the dorsal skin to enable assessment of pain-related responses. In some experiments, T cells were isolated from LNs and spleen of transgenic OT-I/Thy1.1$^{+/+}$/Rag1$^{-/-}$ mice. 10^5~10^6 OT-I cells were adoptively transferred to Thy1.2$^+$ host mice before VACV-OVA infection to study the virus-specific T cell response.

Skin explant assay and ELISA

Mice were shaved at the back and immunized as described. Mice were sacrificed at indicated time points, and 12-mm punch biopsies of the shaved skin were collected and rapidly transferred into a 24-well plate containing 1 ml of serum-free DMEM. Explants were incubated for 30 min at 32°C with gentle rotation (150 rpm) before supernatants were collected for analysis. Mouse SP and CGRP were detected using competitive mouse Substance P and CGRP ELISA kits (both from Cayman Chemical). All procedures were carried out according to the manufacturer's protocols. Samples were assayed in duplicate, and concentrations were determined from a standard curve.

von Frey assay

All animals were acclimatized to the behavioral testing setup for at least three habituation sessions. At least two baseline measures were obtained for each behavioral test before testing. To measure mechanical sensitivity, animals were placed on an elevated wire mesh in individual chambers, and the plantar surface of the hindpaw was stimulated with von Frey monofilaments (range from 0.008 to 2.0 g). The withdrawal threshold was determined as the filament at which the animal withdrew its paw at least five times out of 10 consecutive tests.

Hargreaves paw-withdrawal test

Animals were habituated in individual chambers for at least 1 h with the apparatus powered on prior to testing. Mice were placed on the glass plate of a Hargreaves apparatus (Model 390 G, IITC Life Science). A focused radiant heat source (active intensity 23%) was applied to the plantar surface of the hind paw. Paw-withdrawal latency was defined as the time (in seconds) from stimulus onset to a heat-evoked withdrawal response. To prevent tissue damage, a cutoff latency of 40 s was imposed.

Preparation of cell suspensions

Shaved skin samples (12-mm full-thickness punch biopsies) were processed either as whole skin or separated into epidermal and dermal fractions before digestion. For whole-skin digestion, skin samples were cut into small fragments and incubated in HBSS containing 1 mg/ml collagenase A (11088785103; Roche) and 40 µg/ml DNase I (10104159001; Roche) at 37°C for 1.5 h.

Downloaded from rupress.org/jem/article-pdf/223/12/e20261215/2044247/jem_20261215.pdf by University of California Irvine user on 16 November 2026

Digested tissues were filtered through a 70-µm nylon cell strainer, and cells were collected and washed three times with DMEM supplemented with 10% FBS.

For epidermal and dermal separation, skin samples were first incubated in 4 mg/ml dispase II to separate the epidermis from the dermis. The epidermal sheets were then digested in 0.25% Trypsin-EDTA for 20 min to generate single-cell suspensions. The dermal fractions were cut into small pieces and digested using the same collagenase A/DNase I buffer described for whole-skin digestion (1 mg/ml collagenase A and 40 µg/ml DNase I in HBSS at 37°C for 1.5 h). Cell suspensions were filtered through a 70-µm nylon cell strainer and washed with DMEM containing 10% FBS. After digestion, all skin-derived cells were washed in FACS buffer (2% FBS, 2 mM EDTA, and 0.001% NaN_3) to obtain homogeneous single-cell suspensions prior to staining.

For experiments involving dLN analysis, s.s. was performed in the upper dorsal region, and the bilateral brachial LNs were collected and pooled from each mouse as the dLNs. In some experiments for the DC subset staining, LNs and spleen were subjected to digestion at 37°C in 1 mg/ml collagenase and 40 µg/ml DNase I at 37°C for 30 min before preparation of single-cell suspensions.

Antibodies and flow cytometry

Cells were stained with live/dead at room temperature for 10 min, washed, and stained with an antibody mix in FACS buffer (2% FBS, 2 mM EDTA, and 0.001% NaN_3) for 30 min on ice. The following anti-mouse antibodies and flow cytometry reagents were used; anti-Thy1.1 (BioLegend, clone OX-7, RRID: AB_10899572), anti-CD8a (BD Bioscience, clone 53–6.7, RRID: AB_2739500), anti-CD4 (BioLegend, clone RM4-5, RRID: AB_2563053), anti-TCRb (BioLegend, clone H57-597, RRID: AB_2565655), anti-CD45 (BioLegend, clone 30-F11, RRID: AB_2860600), anti-CD19 (BD Horizon, clone 1D3, RRID: AB_2737915), anti-CD44 (BioLegend, clone IM7, RRID: AB_493681), anti-CD62L (BioLegend, clone MEL-14, RRID: AB_2563058), anti-CD103 (BioLegend, clone H1.2F3, RRID: AB_493564), anti-MHCII (BioLegend, clone M5/114.15.2, RRID: AB_2734168), anti-CD11c (BioLegend, clone N418, RRID: AB_313777), anti-CD207 (BioLegend, clone 4C7, RRID: AB_2561998), anti-XCR1 (BioLegend, clone ZET, RRID: AB_2783119), anti-CD326 (BioLegend, clone G8.8, RRID: AB_2563983), anti-CD103 (BioLegend, clone 2E7, RRID: AB_2686970), anti-CD11b (BioLegend, clone M1/70, RRID: AB_2810328), anti-CD24 (BioLegend, clone M1/69, RRID: AB_2563464), anti-CD301b (BioLegend, clone URA-1, RRID: AB_2563389), anti-CD64 (BioLegend, clone X54-5/7.1, RRID: AB_2735016), anti-CD40 (BioLegend, clone 3/23, RRID: AB_3068198), anti-CD80 (BioLegend, clone 16-10A1, RRID: AB_313132), anti-CD86 (BioLegend, clone GL-1, RRID: AB_493463), anti-CXCR4 (BioLegend, clone L276F12, RRID: AB_2562787), anti-CCR7 (BioLegend, clone 4B12, RRID: AB_389358), anti-CD107a (BioLegend, clone 1D4B, RRID: AB_571983), anti-IFNg (BioLegend, clone XMG1.2, RRID: AB_2650928), anti-TNFa (BioLegend, clone MP6-XT22, RRID: AB_961434), anti-GzmA (eBioscience, clone CB9, RRID: AB_2574331), anti-GzmB (eBioscience, clone NGZB, RRID: AB_10853339), and Zombie live/dead Near Infrared (BioLegend). Flow cytometric data were recorded on Cytek Aurora and analyzed using FlowJo (version 10).

Immunofluorescence microscopy

Mouse skin and DRG samples were fixed in formalin, embedded in paraffin, sectioned, and stored at room temperature until use. For deparaffinization, slides were baked for 20 min at 58°C; cooled to room temperature; washed in xylene for 30 min; and rehydrated in 100, 95, and 75% ethanol and deionized water. Slides were cooled to room temperature, washed in PBS, blocked with protein block (Dako), then stained with primary antibodies diluted in protein block at 4°C overnight and secondary antibodies for 30 min, with two 3-min wash steps between antibodies. Slides were washed in Tris-buffered saline with Tween and deionized water and mounted in Vectashield Hard Set Mounting Medium with DAPI (Vector Laboratories). Tissues were imaged immediately after mounting on a Mantra Quantitative Pathology Workstation or a Leica Stellaris 8 Falcon WLL pp inverted.

Denervation

Chemical ablation of TRPV1-expressing peripheral neurons was performed using RTX according to previously published protocols (Lai et al., 2020). Systemic ablation of Trpv1-expressing neurons was achieved by daily s.c. injection of escalating doses of RTX (Alomone Labs; 30, 70, 100 mg/kg for 3 consecutive days) or vehicle (2% DMSO/0.15% Tween-80/PBS) in the flanks of 4-wk-old C57BL/6 WT mice. RTX-treated mice were allowed to rest for 4–6 wk before use. Loss of $Trpv1^+$ neurons in the DRG was confirmed by reduced thermal responses to noxious heat during hot plate tests (55°C).

In vivo depletion of LC or of Langerin+ dDC

For systemic in vivo depletion of Langerin+ dDC or LC, Lang-DTR mice were injected i.p. with 1 mg DT (Sigma-Aldrich) using the specified timing of administration based on different purposes of the experiment.

Kaede photoconversion

A 2 × 2-cm patch of skin on the back was shaved, followed by application of a chemical depilatory agent (Veet) for 1 min, then removed by multiple washings with PBS. The exposed skin was subjected to violet light (420 nm) using a Bluewave LED visible light curing unit (Dymax) with a 420-nm bandpass filter (Andover Corp). Skin was exposed to this wavelength with the light source at maximum power, ∼7.5 cm away from the skin for 10 min. Following photoconversion, mice were immunized with VACV virus through s.s. in the shaved region as described above. 72 h following immunization, skin dLNs were isolated and analyzed for skin DC migration using flow cytometry.

CGRPα/CGRP8-37 injection

In some instances, CGRPα (RP11095; GenScript) or CGRP8-37 (RP11090; GenScript) was administered intradermally during infection at a total of 0.5 µg per mouse, spread over 5 sites at the infected site (Cohen et al., 2019).

Downloaded from rupress.org/jem/article-pdf/223/12/e20261215/2044247/jem_20261215.pdf by University of California Irvine user on 16 November 2026

T cell ex vivo functional assay

$CD8^+$ T cells were enriched from spleens using a $CD8^+$ T Cell Isolation Kit (Miltenyi Biotec) to increase purity. Enriched cells were stained with antibodies against CD8α, CD4, TCRβ, CD19, Thy1.1, and CD45, and $CD8\alpha^+Thy1.1^+CD44^+CD62L^+$ T cells were subsequently purified by fluorescence-activated cell sorting using an Aurora cell sorter at the Harvard Medical School Flow Cytometry Core Facility. Sorted $CD8^+$ T cells were co-cultured with naïve splenocytes at a 1:5 ratio and stimulated for 3 h at 37°C in DMEM supplemented with 10% (vol/vol) bovine growth serum and 10 nM SIINFEKL peptide. Brefeldin A (5 µg/ml) was added after the first hour of stimulation to allow intracellular cytokine accumulation. To assess degranulation, anti-CD107a antibody (clone 1D4B, BD Biosciences) was included for the duration of the stimulation. Following stimulation, cells were processed for intracellular staining using the Foxp3/Transcription Factor Fixation/Permeabilization Kit (eBioscience), according to the manufacturer's instructions.

Transwell migration assay

The migration assay was performed using 24-well Transwell plates containing 8-µm-pore size polycarbonate filters (Corning, Life Science). Skin epidermis was separated from dermis after incubating with dispase II at 4°C overnight. Epidermis was cut into small pieces and then digested with 0.25% Trypsin-EDTA for 20 min at 37°C. The cell concentration of epidermal cells was adjusted with DMEM medium, and 10^6 cells were added to the upper chambers and 600 µl of DMEM medium to the lower chambers. Depending on the purpose of the experiment, 50 nM of recombinant murine CXCL12 (250-20A; PeproTech), 1 nM CGRP (GenScript), or vehicle was added to the lower chamber, which was then incubated at 37°C in a 5% CO_2 incubator for 48 h. Cells from the lower chamber were subsequently collected. Flow cytometry was performed to detect the number of cells migrating into the lower chamber of LCs.

Bulk RNA-seq and data analysis

DCs from skin dLNs were first purified using the Pan Dendritic Cell Isolation kit (Miltenyi) to get higher purity. Cells were then stained with anti-CD11c, anti-MHCI, anti-CD207, anti-CD103, anti-CD326, and anti-CD45, and subsequently sorted the $Langerin^+CD326^+$ DC population using a FACSAria Cell Sorter (Becton-Dickinson) at Beth Israel Deaconess Medical Center Flow Cytometry Core Facilities. Purity of sorted cell populations was over 98% as measured by flow cytometry. Total RNA was extracted with the RNeasy Micro Kit (Qiagen) in accordance with the manufacturer's protocol. cDNA was synthesized using Takara SmartSeq version 4 reagents. Full-length cDNA was fragmented to a mean size of 200 bp with a Covaris R230 ultrasonicator, and Illumina sequencing libraries were prepared from 2 ng of sheared cDNA using IDT DNAseq library prep reagents on a Beckman Coulter Biomek i7 according to the manufacturer's protocol. The finished dsDNA libraries were quantified by Qubit fluorometer and Agilent TapeStation 2200. Uniquely dual-indexed libraries were pooled in equimolar ratios and evaluated for cluster efficiency and pool balance with shallow sequencing on an Illumina MiSeq. Final sequencing was performed on an Illumina NovaSeq X Plus with paired-end 150 bp reads at the Dana-Farber Cancer Institute Molecular Biology Core Facilities. Transcript quantification was performed using Salmon, and differential expression analysis was conducted in R (version 4.4.2) using DESeq2 (version 1.46.0). Genes were considered differentially expressed for P value <0.05 and $|\log2FC| > 1$. For clustering and visualization, gene expression counts were first normalized using the variance-stabilizing transformation in DESeq2. The transformed values were then centered and scaled per gene (Z-score normalization) before heatmap generation. The heatmap was generated using the ComplexHeatmap package (version 2.22.0) in R. Both genes and samples were hierarchically clustered using Euclidean distance and the complete linkage method.

Statistical analysis

Statistical analysis of results was performed using GraphPad Prism 7–8 (GraphPad Software). Multiple Mann–Whitney tests, ordinary one-way ANOVA, or two-way ANOVA were applied as indicated in figure legends. Statistical significance was considered for P values <0.05. Details are listed in the respective figure legends.

Online supplemental material

Fig. S1 shows data related to Fig. 1, including the kinetics of VACV s.s.-induced pain, tissue swelling, sensory neuron activation, and CGRP release, as well as the effects of nociceptor ablation. Fig. S2 shows data related to Fig. 2, including primary antiviral $CD8^+$ T cell responses in the spleen and LNs following genetic or pharmacological ablation of nociceptor neurons, as well as $CD69^+CD103^+$ memory OT-I T cells in the skin. Fig. S3 shows data related to Figs. 3 and 4, including the effects of CGRPα and CGRP8-37 on primary effector $CD8^+$ T cell responses, the contribution of central memory T cells to viral clearance, and Ramp1 expression across skin cell populations. Fig. S4 shows data related to Fig. 5, including migDC subsets and co-stimulatory molecule expression in migrating LCs in nociceptor- and RAMP1-deficient mice, as well as the effect of T cell–intrinsic Ramp1 deficiency on memory $CD8^+$ T cell responses. Fig. S5 shows data related to Fig. 6, including the efficiency and specificity of LC^+ depletion, transcriptional profiling of migrating LCs from *Ramp1*$^{+/+}$ and *Ramp1*$^{-/-}$ mice, and analysis of CCR7 and CXCR4 expression associated with LC migration. Table S1 shows bulk RNA-sequencing data from migratory Langerhans cells isolated from immunized mice.

Data availability

This paper does not report original code. The sequencing data generated in this study are available through the NCBI Gene Expression Omnibus under accession number GSE344957 and will be publicly available upon publication. All data reported in this paper will be shared by the lead contact upon request. Any additional information required to reanalyze the data reported in this paper is available from the lead contact upon request.

Downloaded from rupress.org/jem/article-pdf/223/12/e20261215/2044247/jem_20261215.pdf by University of California Irvine user on 16 November 2026

Acknowledgments

We thank all members of the Department of Dermatology for helpful discussions. We thank the Brigham and Women's Hospital Center for Comparative Medicine for animal housing, Brigham and Women's Hospital Pathology Cores (Harvard Cancer Center): BWH Pathology Cores (HCC) for tissue embedding and slide preparation, Beth Israel Deaconess Medical Center Flow Cytometry Core for cell sorting, and Molecular Biology Core Facilities at Dana-Farber Cancer Institute for RNA library preparation and sequencing.

This study was supported by the National Institute of Health grants R01 AR065807 (T.S. Kupper), AI175582 (T.S. Kupper), 5R01AI168005 (I.M. Chiu), and P30AR069625-06 (R.A. Clark); the Food Allergy Science Initiative 2024-FASI-NEURO-HM24315 (I.M. Chiu); and National Science Foundation grant CBET2134916 (S.X. Atwood and Y.Y. Jia).

Author contributions: Jiang Zhang: conceptualization, data curation, formal analysis, investigation, methodology, project administration, resources, supervision, validation, visualization, and writing—original draft, review, and editing. Timothy Y. Pan: investigation. Alexander L. Kley: investigation, resources, and writing—review and editing. Bharat Ashok Rajmalani: investigation and resources. Jason B. Williams: conceptualization, methodology, and resources. Marine-Alexia Lefevre: formal analysis, visualization, and writing—review and editing. Xiaopeng Fu: investigation and validation. Qian Zhan: investigation and resources. Liwen Deng: investigation and methodology. Yunlong Y. Jia: formal analysis, resources, validation, and writing—review and editing. Kyle Deans: investigation and resources. Yu Yan: investigation and writing—review and editing. Yunhao Zhai: methodology, resources, and writing—review and editing. Ozge Erdogan: investigation, methodology, and writing—review and editing. Samantha Choi: methodology and project administration. Calvin Wong: methodology and writing—review and editing. Scott X. Atwood: formal analysis, funding acquisition, and writing—review and editing. Rachael A. Clark: methodology and resources. Isaac M. Chiu: conceptualization, funding acquisition, project administration, supervision, and writing—review and editing. Thomas S. Kupper: conceptualization, formal analysis, funding acquisition, project administration, and writing—review and editing.

Disclosures: I.M. Chiu reported grants from HV Biome and Allergan, and personal fees from H-ventures, Fzata, Nilo Inc., and Panther outside the submitted work. No other disclosures were reported.

Submitted: 1 July 2026
Revised: 10 September 2026
Accepted: 2 October 2026

References

Abraira, V.E., and D.D. Ginty. 2013. The sensory neurons of touch. *Neuron*. 79: 618–639. https://doi.org/10.1016/j.neuron.2013.07.051

Achanta, S., N.R. Chintagari, M. Brackmann, S. Balakrishna, and S.-E. Jordt. 2018. TRPA1 and CGRP antagonists counteract vesicant-induced skin injury and inflammation. *Toxicol. Lett.* 293:140–148. https://doi.org/10.1016/j.toxlet.2018.03.007

Allan, R.S., C.M. Smith, G.T. Belz, A.L. van Lint, L.M. Wakim, W.R. Heath, and F.R. Carbone. 2003. Epidermal viral immunity induced by CD8alpha+ dendritic cells but not by Langerhans cells. *Science*. 301:1925–1928. https://doi.org/10.1126/science.1087576

Balood, M., M. Ahmadi, T. Eichwald, A. Ahmadi, A. Majdoubi, K. Roversi, K. Roversi, C.T. Lucido, A.C. Restaino, S. Huang, et al. 2022. Nociceptor neurons affect cancer immunosurveillance. *Nature*. 611:405–412. https://doi.org/10.1038/s41586-022-05374-w

Baral, P., S. Udit, and I.M. Chiu. 2019. Pain and immunity: Implications for host defence. *Nat. Rev. Immunol.* 19:433–447. https://doi.org/10.1038/s41577-019-0147-2

Basbaum, A.I., D.M. Bautista, G. Scherrer, and D. Julius. 2009. Cellular and molecular mechanisms of pain. *Cell*. 139:267–284. https://doi.org/10.1016/j.cell.2009.09.028

Blake, K.J., X.R. Jiang, and I.M. Chiu. 2019. Neuronal regulation of immunity in the skin and lungs. *Trends Neurosciences*. 42:537–551. https://doi.org/10.1016/j.tins.2019.05.005

Brain, S.D., T.J. Williams, J.R. Tippins, H.R. Morris, and I. MacIntyre. 1985. Calcitonin gene-related peptide is a potent vasodilator. *Nature*. 313: 54–56. https://doi.org/10.1038/313054a0

Bursch, L.S., L. Wang, B. Igyarto, A. Kissenpfennig, B. Malissen, D.H. Kaplan, and K.A. Hogquist. 2007. Identification of a novel population of Langerin+ dendritic cells. *J. Exp. Med.* 204:3147–3156. https://doi.org/10.1084/jem.20071966

Cabeza-Cabrerizo, M., A. Cardoso, C.M. Minutti, M. Pereira da Costa, and C. Reis e Sousa. 2021. Dendritic cells revisited. *Annu. Rev. Immunol.* 39: 131–166. https://doi.org/10.1146/annurev-immunol-061020-053707

Cañedo-Dorantes, L., and M. Cañedo-Ayala. 2019. Skin acute wound healing: A comprehensive review. *Int. J. Inflamm.* 2019:3706315. https://doi.org/10.1155/2019/3706315

Chiu, I.M., B.A. Heesters, N. Ghasemlou, C.A. Von Hehn, F. Zhao, J. Tran, B. Wainger, A. Strominger, S. Muralidharan, A.R. Horswill, et al. 2013. Bacteria activate sensory neurons that modulate pain and inflammation. *Nature*. 510:52–57. https://doi.org/10.1038/nature12479

Chu, C., D. Artis, and I.M. Chiu. 2020. Neuro-immune interactions in the tissues. *Immunity*. 52:464–474. https://doi.org/10.1016/j.immuni.2020.02.017

Cohen, J.A., T.N. Edwards, A.W. Liu, T. Hirai, M.R. Jones, J. Wu, Y. Li, S. Zhang, J. Ho, B.M. Davis, et al. 2019. Cutaneous TRPV1+ neurons trigger protective innate type 17 anticipatory immunity. *Cell*. 178:919–932.e14. https://doi.org/10.1016/j.cell.2019.06.022

Cole, S.W., B.D. Jamieson, and J.A. Zack. 1999. cAMP up-regulates cell surface expression of lymphocyte CXCR4: Implications for chemotaxis and HIV-1 infection. *J. Immunol.* 162:1392–1400. https://doi.org/10.4049/jimmunol.162.3.1392

Deng, L., J.E. Gillis, I.M. Chiu, and D.H. Kaplan. 2024. Sensory neurons: An integrated component of innate immunity. *Immunity*. 57:815–831. https://doi.org/10.1016/j.immuni.2024.03.008

Filtjens, J., A. Roger, L. Quatrini, E. Wieduwild, J. Gouilly, G. Hoeffel, R. Rossignol, C. Daher, G. Debroas, S. Henri, et al. 2021. Nociceptive sensory neurons promote CD8 T cell responses to HSV-1 infection. *Nat. Commun.* 12:2936. https://doi.org/10.1038/s41467-021-22841-6

Frutos, A.M., S. Cleary, E.L. Reeves, H.M. Ahmad, A.M. Price, W.H. Self, Y. Zhu, B. Safdar, I.D. Peltan, K.W. Gibbs, et al. 2025. Interim estimates of 2024–2025 seasonal influenza vaccine effectiveness — Four vaccine effectiveness networks, United States, October 2024–February 2025. *MMWR Morb. Mortal. Wkly. Rep.* 74:83–90. https://doi.org/10.15585/mmwr.mm7406a2

Gao, Y.-J., and R.-R. Ji. 2009. c-Fos and pERK, which is a better marker for neuronal activation and central sensitization after noxious stimulation and tissue injury? *Open Pain J.* 2:11–17. https://doi.org/10.2174/1876386300902010011

Gouin, O., K. L'Herondelle, N. Lebonvallet, C. Le Gall-Ianotto, M. Sakka, V. Buhé, E. Plée-Gautier, J.-L. Carré, L. Lefeuvre, L. Misery, and R. Le Garrec. 2017. TRPV1 and TRPA1 in cutaneous neurogenic and chronic inflammation: Pro-inflammatory response induced by their activation and their sensitization. *Protein Cell*. 8:644–661. https://doi.org/10.1007/s13238-017-0395-5

Harbour, J.C., M. Abdelbary, J.B. Schell, S.P. Fancher, J.J. McLean, T.J. Nappi, S. Liu, T.J. Nice, Z. Xia, K. Früh, and J.C. Nolz. 2023. T helper 1 effector memory CD4+ T cells protect the skin from poxvirus infection. *Cell Rep.* 42:112407. https://doi.org/10.1016/j.celrep.2023.112407

Heipertz, E.L., M.L. Davies, E. Lin, and C.C. Norbury. 2014. Prolonged antigen presentation following an acute virus infection requires direct and then

Downloaded from rupress.org/jem/article-pdf/223/12/e20261215/2044247/jem_20261215.pdf by University of California Irvine user on 16 November 2026

cross-presentation. *J. Immunol.* 193:4169–4177. https://doi.org/10.4049/jimmunol.1302565
Henri, S., L.F. Poulin, S. Tamoutounour, L. Ardouin, M. Guilliams, B. de Bovis, E. Devilard, C. Viret, H. Azukizawa, A. Kissenpfennig, and B. Malissen. 2010. CD207+ CD103+ dermal dendritic cells cross-present keratinocyte-derived antigens irrespective of the presence of Langerhans cells. *J. Exp. Med.* 207:189–206. https://doi.org/10.1084/jem.20091964
Hosoi, J., G.F. Murphy, C.L. Egan, E.A. Lerner, S. Grabbe, A. Asahina, and R.D. Granstein. 1993a. Regulation of Langerhans cell function by nerves containing calcitonin gene-related peptide. *Nature*. 363:159–163. https://doi.org/10.1038/363159a0
Hosoi, J., G.F. Murphy, C.L. Egan, E.A. Lerner, S. Grabbe, A. Asahina, and R.D. Granstein. 1993b. Regulation of Langerhans cell function by nerves containing calcitonin gene-related peptide. *Nature*. 363:159–163. https://doi.org/10.1038/363159a0
Hou, Y., L. Sun, M.W. LaFleur, L. Huang, C. Lambden, P.I. Thakore, K. Geiger-Schuller, K. Kimura, L. Yan, Y. Zang, et al. 2024. Neuropeptide signalling orchestrates T cell differentiation. *Nature*. 635:444–452. https://doi.org/10.1038/s41586-024-08049-w
Huang, X., S. Ao, R. Xu, X. Gao, S. Qi, Y. Liang, P. Feng, R. Xue, Y. Ren, J. Han, et al. 2025. Sensory neuroimmune signaling in the pathogenesis of Stevens-Johnson syndrome and toxic epidermal necrolysis. *J. Allergy Clin. Immunol.* 155:533–546. https://doi.org/10.1016/j.jaci.2024.10.015
Huh, J.R., and H. Veiga-Fernandes. 2020. Neuroimmune circuits in inter-organ communication. *Nat. Rev. Immunol.* 20:217–228. https://doi.org/10.1038/s41577-019-0247-z
Jacobs, B.L., J.O. Langland, K.V. Kibler, K.L. Denzler, S.D. White, S.A. Holechek, S. Wong, T. Huynh, and C.R. Baskin. 2009. Vaccinia virus vaccines: Past, present and future. *Antiviral Res.* 84:1–13. https://doi.org/10.1016/j.antiviral.2009.06.006
Jiang, X., R.A. Clark, L. Liu, A.J. Wagers, R.C. Fuhlbrigge, and T.S. Kupper. 2012. Skin infection generates non-migratory memory CD8+ TRM cells providing global skin immunity. *Nature*. 483:227–231. https://doi.org/10.1038/nature10851
Kabashima, K., N. Shiraishi, K. Sugita, T. Mori, A. Onoue, M. Kobayashi, J. Sakabe, R. Yoshiki, H. Tamamura, N. Fujii, et al. 2007. CXCL12-CXCR4 engagement is required for migration of cutaneous dendritic cells. *Am. J. Pathol.* 171:1249–1257. https://doi.org/10.2353/ajpath.2007.070225
Kashem, S.W., M. Haniffa, and D.H. Kaplan. 2017. Antigen-presenting cells in the skin. *Annu. Rev. Immunol.* 35:469–499. https://doi.org/10.1146/annurev-immunol-051116-052215
Kashem, S.W., M.S. Riedl, C. Yao, C.N. Honda, L. Vulchanova, and D.H. Kaplan. 2015. Nociceptive sensory fibers drive interleukin-23 production from CD301b+ dermal dendritic cells and drive protective cutaneous immunity. *Immunity*. 43:515–526. https://doi.org/10.1016/j.immuni.2015.08.016
Kissenpfennig, A., S. Henri, B. Dubois, C. Laplace-Builhé, P. Perrin, N. Romani, C.H. Tripp, P. Douillard, L. Leserman, D. Kaiserlian, et al. 2005. Dynamics and function of Langerhans cells in vivo. *Immunity*. 22:643–654. https://doi.org/10.1016/j.immuni.2005.04.004
Kohlmeier, J.E., and D.L. Woodland. 2009. Immunity to respiratory viruses. *Annu. Rev. Immunol.* 27:61–82. https://doi.org/10.1146/annurev.immunol.021908.132625
Kulalert, W., A.C. Wells, V.M. Link, A.I. Lim, N. Bouladoux, M. Nagai, O.J. Harrison, O. Kamenyeva, J. Kabat, M. Enamorado, et al. 2024. The neuroimmune CGRP–RAMP1 axis tunes cutaneous adaptive immunity to the microbiota. *Proc. Natl. Acad. Sci. USA*. 121:e2322574121. https://doi.org/10.1073/pnas.2322574121
Kupari, J., and P. Ernfors. 2023. Molecular taxonomy of nociceptors and pruriceptors. *Pain*. 164:1245–1257. https://doi.org/10.1097/j.pain.0000000000002831
Lai, N.Y., M.A. Musser, F.A. Pinho-Ribeiro, P. Baral, A. Jacobson, P. Ma, D.E. Potts, Z. Chen, D. Paik, S. Soualhi, et al. 2020. Gut-innervating nociceptor neurons regulate peyer's patch microfold cells and SFB levels to mediate Salmonella host defense. *Cell*. 180:33–49.e22. https://doi.org/10.1016/j.cell.2019.11.014
Liu, L., Q. Zhong, T. Tian, K. Dubin, S.K. Athale, and T.S. Kupper. 2010. Epidermal injury and infection during poxvirus immunization is crucial for the generation of highly protective T cell–mediated immunity. *Nat. Med.* 16:224–227. https://doi.org/10.1038/nm.2078
Mackay, L.K., A. Rahimpour, J.Z. Ma, N. Collins, A.T. Stock, M.-L. Hafon, J. Vega-Ramos, P. Lauzurica, S.N. Mueller, T. Stefanovic, et al. 2013. The developmental pathway for CD103+CD8+ tissue-resident memory T cells of skin. *Nat. Immunol.* 14:1294–1301. https://doi.org/10.1038/ni.2744
Mackay, L.K., A.T. Stock, J.Z. Ma, C.M. Jones, S.J. Kent, S.N. Mueller, W.R. Heath, F.R. Carbone, and T. Gebhardt. 2012. Long-lived epithelial immunity by tissue-resident memory T (TRM) cells in the absence of persisting local antigen presentation. *Proc. Natl. Acad. Sci. USA*. 109:7037–7042. https://doi.org/10.1073/pnas.1202288109
Malissen, B., S. Tamoutounour, and S. Henri. 2014. The origins and functions of dendritic cells and macrophages in the skin. *Nat. Rev. Immunol.* 14:417–428. https://doi.org/10.1038/nri3683
Mikami, N., H. Matsushita, T. Kato, R. Kawasaki, T. Sawazaki, T. Kishimoto, Y. Ogitani, K. Watanabe, Y. Miyagi, K. Sueda, et al. 2011. Calcitonin gene-related peptide is an important regulator of cutaneous immunity: Effect on dendritic cell and T cell functions. *J. Immunol.* 186:6886–6893. https://doi.org/10.4049/jimmunol.1100028
Mishra, S.K., and M.A. Hoon. 2010. Ablation of TrpV1 neurons reveals their selective role in thermal pain sensation. *Mol. Cell Neurosci.* 43:157–163. https://doi.org/10.1016/j.mcn.2009.10.006
Mishra, S.K., S.M. Tisel, P. Orestes, S.K. Bhangoo, and M.A. Hoon. 2011. TRPV1-lineage neurons are required for thermal sensation. *EMBO J.* 30:582–593. https://doi.org/10.1038/emboj.2010.325
Pan, Y., L. Liu, T. Tian, J. Zhao, C.K. Park, S.Y. Lofftus, C.A. Stingley, Y. Yan, S. Mei, X. Liu, et al. 2021. Epicutaneous immunization with modified vaccinia Ankara viral vectors generates superior T cell immunity against a respiratory viral challenge. *NPJ Vaccines*. 6:1. https://doi.org/10.1038/s41541-020-00265-5
Park, C.O., X. Fu, X. Jiang, Y. Pan, J.E. Teague, N. Collins, T. Tian, J.T. O'Malley, R.O. Emerson, J.H. Kim, et al. 2018. Staged development of long-lived T-cell receptor αβ T H 17 resident memory T-cell population to *Candida albicans* after skin infection. *J. Allergy Clin. Immunol.* 142:647–662. https://doi.org/10.1016/j.jaci.2017.09.042[
Pavlov, V.A., and K.J. Tracey. 2017. Neural regulation of immunity: Molecular mechanisms and clinical translation. *Nat. Neurosci.* 20:156–166. https://doi.org/10.1038/nn.4477
Perner, C., C.H. Flayer, X. Zhu, P.A. Aderhold, Z.N.A. Dewan, T. Voisin, R.B. Camire, O.A. Chow, I.M. Chiu, and C.L. Sokol. 2020. Substance P release by sensory neurons triggers dendritic cell migration and initiates the type-2 immune response to allergens. *Immunity*. 53:1063–1077.e7. https://doi.org/10.1016/j.immuni.2020.10.001
Pinho-Ribeiro, F.A., B. Baddal, R. Haarsma, M. O'Seaghdha, N.J. Yang, K.J. Blake, M. Portley, W.A. Verri, J.B. Dale, M.R. Wessels, and I.M. Chiu. 2018. Blocking neuronal signaling to immune cells treats streptococcal invasive infection. *Cell*. 173:1083–1097.e22. https://doi.org/10.1016/j.cell.2018.04.006
Redpath, A.N., M. François, S.-P. Wong, D. Bonnet, and S.M. Rankin. 2017. Two distinct CXCR4 antagonists mobilize progenitor cells in mice by different mechanisms. *Blood Adv.* 1:1934–1943. https://doi.org/10.1182/bloodadvances.2017006064
Roger, A., A. Reynders, G. Hoeffel, and S. Ugolini. 2022. Neuroimmune crosstalk in the skin: A delicate balance governing inflammatory processes. *Curr. Opin. Immunol.* 77:102212. https://doi.org/10.1016/j.coi.2022.102212
Rotrosen, E., and T.S. Kupper. 2023. Assessing the generation of tissue resident memory T cells by vaccines. *Nat. Rev. Immunol.* 23:655. https://doi.org/10.1038/s41577-023-00853-1
Russell, F.A., R. King, S.-J. Smillie, X. Kodji, and S.D. Brain. 2014. Calcitonin gene-related peptide: Physiology and pathophysiology. *Physiol. Rev.* 94:1099–1142. https://doi.org/10.1152/physrev.00034.2013
Schmelz, M., and L.J. Petersen. 2001. Neurogenic inflammation in human and rodent skin. *Physiology*. 16:33–37. https://doi.org/10.1152/physiologyonline.2001.16.1.33
Serhan, N., L. Basso, R. Sibilano, C. Petitfils, J. Meixiong, C. Bonnart, L.L. Reber, T. Marichal, P. Starkl, N. Cenac, et al. 2019. House dust mites activate nociceptor–mast cell clusters to drive type 2 skin inflammation. *Nat. Immunol.* 20:1435–1443. https://doi.org/10.1038/s41590-019-0493-z
Shurin, M.R., G.V. Shurin, S.B. Zlotnikov, and Y.L. Bunimovich. 2020. The neuroimmune Axis in the tumor microenvironment. *J.I.* 204:280–285. https://doi.org/10.4049/jimmunol.1900828
Tamoutounour, S., M. Guilliams, F. Montanana Sanchis, H. Liu, D. Terhorst, C. Malosse, E. Pollet, L. Ardouin, H. Luche, C. Sanchez, et al. 2013. Origins and functional specialization of macrophages and of conventional and monocyte-derived dendritic cells in mouse skin. *Immunity*. 39:925–938. https://doi.org/10.1016/j.immuni.2013.10.004
Tender, G.C., S. Walbridge, Z. Olah, L. Karai, M. Iadarola, E.H. Oldfield, and R.R. Lonser. 2005. Selective ablation of nociceptive neurons for elimination of hyperalgesia and neurogenic inflammation. *J. Neurosurg.* 102:522–525. https://doi.org/10.3171/jns.2005.102.3.0522

Downloaded from rupress.org/jem/article-pdf/223/12/e20261215/2044247/jem_20261215.pdf by University of California Irvine user on 16 November 2026

Thrane, K., M.C.G. Winge, H. Wang, L. Chen, M.G. Guo, A. Andersson, X.M. Abalo, X. Yang, D.S. Kim, S.K. Longo, et al. 2023. Single-cell and spatial transcriptomic analysis of human skin delineates intercellular communication and pathogenic cells. *J. Invest. Dermatol.* 143:2177–2192.e13. https://doi.org/10.1016/j.jid.2023.02.040

Wang, Y., X. Zhang, S. Liu, Z. Gu, Z. Sun, Y. Zang, X. Huang, Y. Wang, Q. Wang, Q. Lin, et al. 2025. Bi-directional communication between intrinsic enteric neurons and ILC2s inhibits host defense against helminth infection. *Immunity*. 58:465–480.e8. https://doi.org/10.1016/j.immuni.2025.01.004

Wang, Z., K. Song, B.S. Kim, and J. Manion. 2024. Sensory neuroimmune interactions at the barrier. *Mucosal Immunol.* 17:1151–1160. https://doi.org/10.1016/j.mucimm.2024.10.001

Wherry, E.J., V. Teichgräber, T.C. Becker, D. Masopust, S.M. Kaech, R. Antia, U.H. von Andrian, and R. Ahmed. 2003. Lineage relationship and protective immunity of memory CD8 T cell subsets. *Nat. Immunol.* 4: 225–234. https://doi.org/10.1038/ni889

Wu, M., G. Song, J. Li, Z. Song, B. Zhao, L. Liang, W. Li, H. Hu, H. Tu, S. Li, et al. 2024. Innervation of nociceptor neurons in the spleen promotes germinal center responses and humoral immunity. *Cell*. 187:2935–2951.e19. https://doi.org/10.1016/j.cell.2024.04.027

Xu, R.-H., S. Remakus, X. Ma, F. Roscoe, and L.J. Sigal. 2010. Direct presentation is sufficient for an efficient anti-viral CD8+ T cell response. *PLoS Pathog.* 6:e1000768. https://doi.org/10.1371/journal.ppat.1000768

Zhang, C., L. Ye, Q. Zhang, F. Wu, and L. Wang. 2020. The role of TRPV1 channels in atherosclerosis. *Channels*. 14:141–150. https://doi.org/10.1080/19336950.2020.1747803

Zhu, Y., K.A. Meerschaert, S. Galvan-Pena, N.-R. Bin, D. Yang, H. Basu, R. Kawamoto, A. Shalaby, S.D. Liberles, D. Mathis, et al. 2024. A chemogenetic screen reveals that Trpv1-expressing neurons control regulatory T cells in the gut. *Science*. 385:eadk1679. https://doi.org/10.1126/science.adk1679

Downloaded from rupress.org/jem/article-pdf/223/12/e20261215/2044247/jem_20261215.pdf by University of California Irvine user on 16 November 2026

JEM

Supplemental material

Downloaded from rupress.org/jem/article-pdf/223/12/e20261215/2044247/jem_20261215.pdf by University of California Irvine user on 16 November 2026

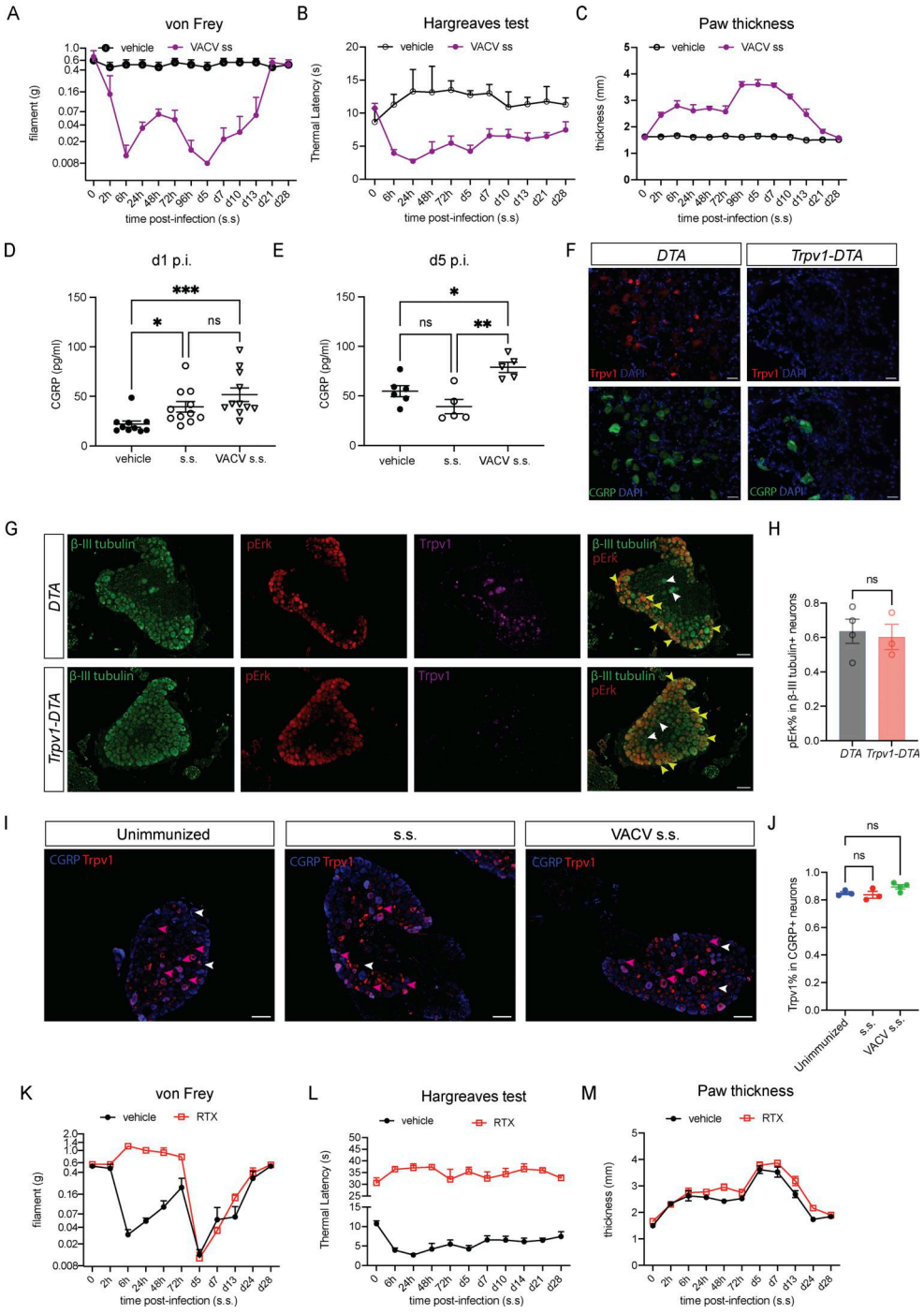

Figure S1. **Long-term effect of pain and CGRP release in mice immunized with VACV via s.s. (A–C)** s.s. on mouse hindpaw (VACV s.s.) induces (A) mechanical hypersensitivity measured using von Frey filaments, (B) thermal hypersensitivity measured using the Hargreaves test, and (C) tissue swelling observed following VACV s.s. from day 0 to day 28 after infection. *N* = 3–4 mice per group, representative of two independent experiments. **(D–E)** CGRP release from VACV-infected (VACV s.s.), s.s. only (s.s.), and vehicle ctrl (vehicle) skin (D) 1 day and (E) 5 days after treatment. Data in D are from *n* = 10-11 mice per group pooled from two independent experiments; data in E are from 5 to 6 mice per group representative of two independent experiments. **(F)** Representative images of CGRP and Trpv1 expression in the DRGs of *DTA* and *Trpv1-DTA* mice. Scale bar, 20 µm. **(G)** Representative immunofluorescence images of DRG from mice 1 day after VACV delivery via s.s. Sections were stained for βIII-tubulin (green), pERK (red), and TRPV1 (magenta). Scale bar, 50 µm. **(H)** Quantification of the percentage of pERK⁺ neurons among βIII-tubulin⁺ DRG neurons following VACV delivery by the indicated routes. **(I)** Representative images of CGRP (blue) and Trpv1 (red) expression in DRG from mice treated with PBS or VACV via s.s. Images were acquired 1 day after treatment, with each data point used representing a single mouse. Scale bars, 50 µm. **(J)** Quantification of the percentage of Trpv1⁺ neurons among CGRP⁺ DRG neurons following VACV delivery. *N* = 3–4 mice per group from one experiment. **(K–M)** VACV s.s. (hindpaw)-induced (K) mechanical pain, (L) thermal pain, and (M) tissue swelling observed between vehicle and RTX-treated groups from day 0 to day 28 after infection. *N* = 4–5 mice per group, representative of two independent experiments. Ordinary one-way ANOVA test (D, E, and J) and Mann–Whitney test with multiple comparisons (G) were used for statistical comparisons, with significance denoted as *P < 0.05, **P < 0.01, ***P < 0.001, and "ns" indicating not significant. Error bars represent mean ± SEM.

Downloaded from rupress.org/jem/article-pdf/223/12/e20261215/2044247/jem_20261215.pdf by University of California Irvine user on 16 November 2026

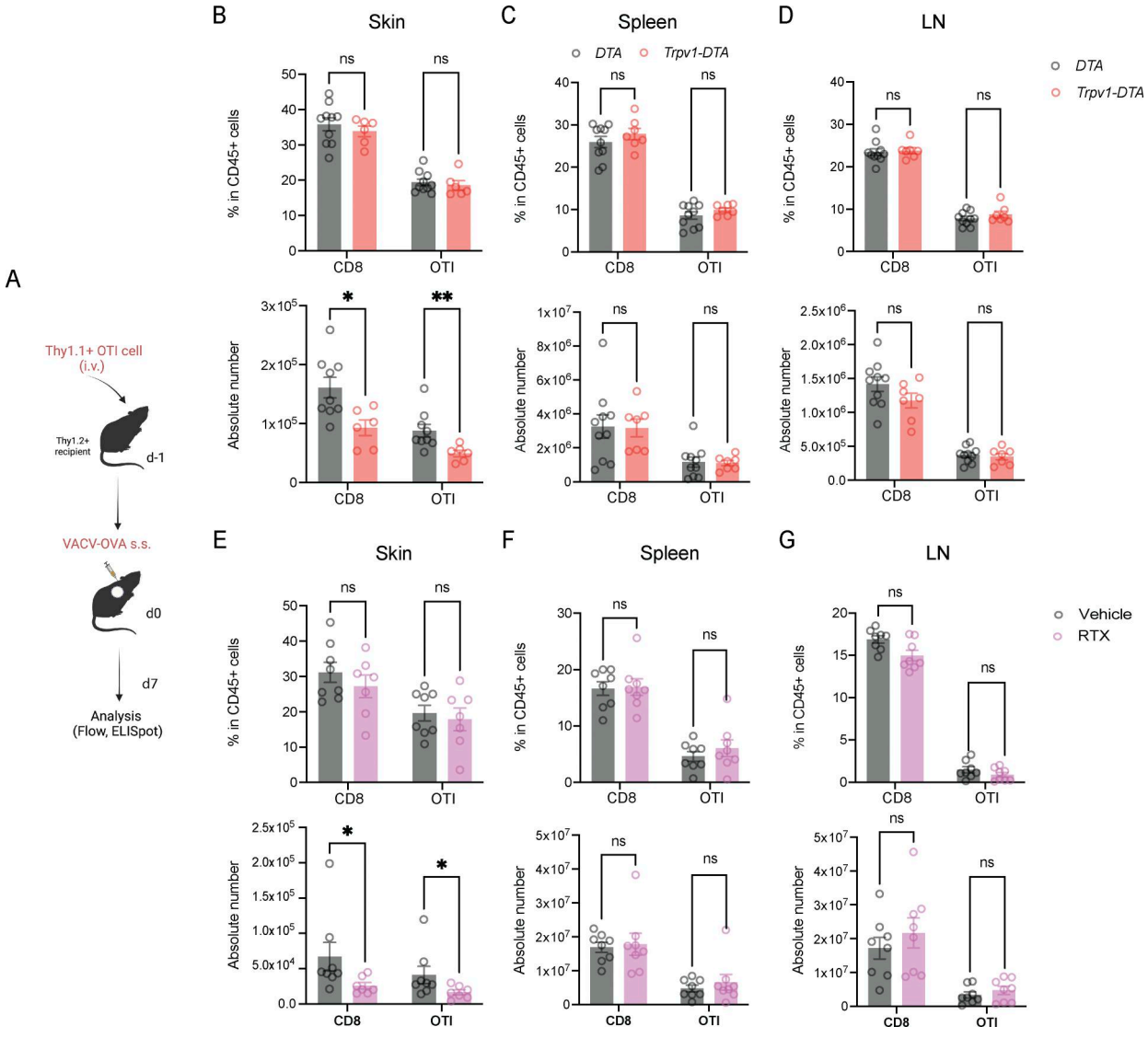

Figure S2. **Ablation of nociceptor neurons does not affect the antiviral CD8 T cell response in the spleen or LN at the primary effector stage.** **(A)** Experimental design used for monitoring antiviral CD8 T cell response in vivo. Thy1.2$^+$ recipient mice were transferred with naïve Thy1.1$^+$ OT-I cells 1 day prior to VACV-OVA infection by s.s. **(B–G)** Percentages and absolute numbers of total and virus-specific CD8$^+$ T cells in the skin, spleen, and LN were determined on day 7 after infection from (B–D) *DTA* and *Trpv1-DTA* mice and from (E–G) DMSO- and RTX-treated mice. Data in B–D are from N = 6–10 mice per group pooled from two independent experiments; data in E–G are from n = 8 mice per group pooled from two independent experiments. Multiple Mann–Whitney tests were used for statistical comparisons (B–G), with significance denoted as *P < 0.05, **P < 0.01, and "ns" indicating not significant. Error bars represent mean ± SEM. **(A)** Figure adapted from an image created in BioRender.

Downloaded from rupress.org/jem/article-pdf/223/12/e20261215/2044247/jem_20261215.pdf by University of California Irvine user on 16 November 2026

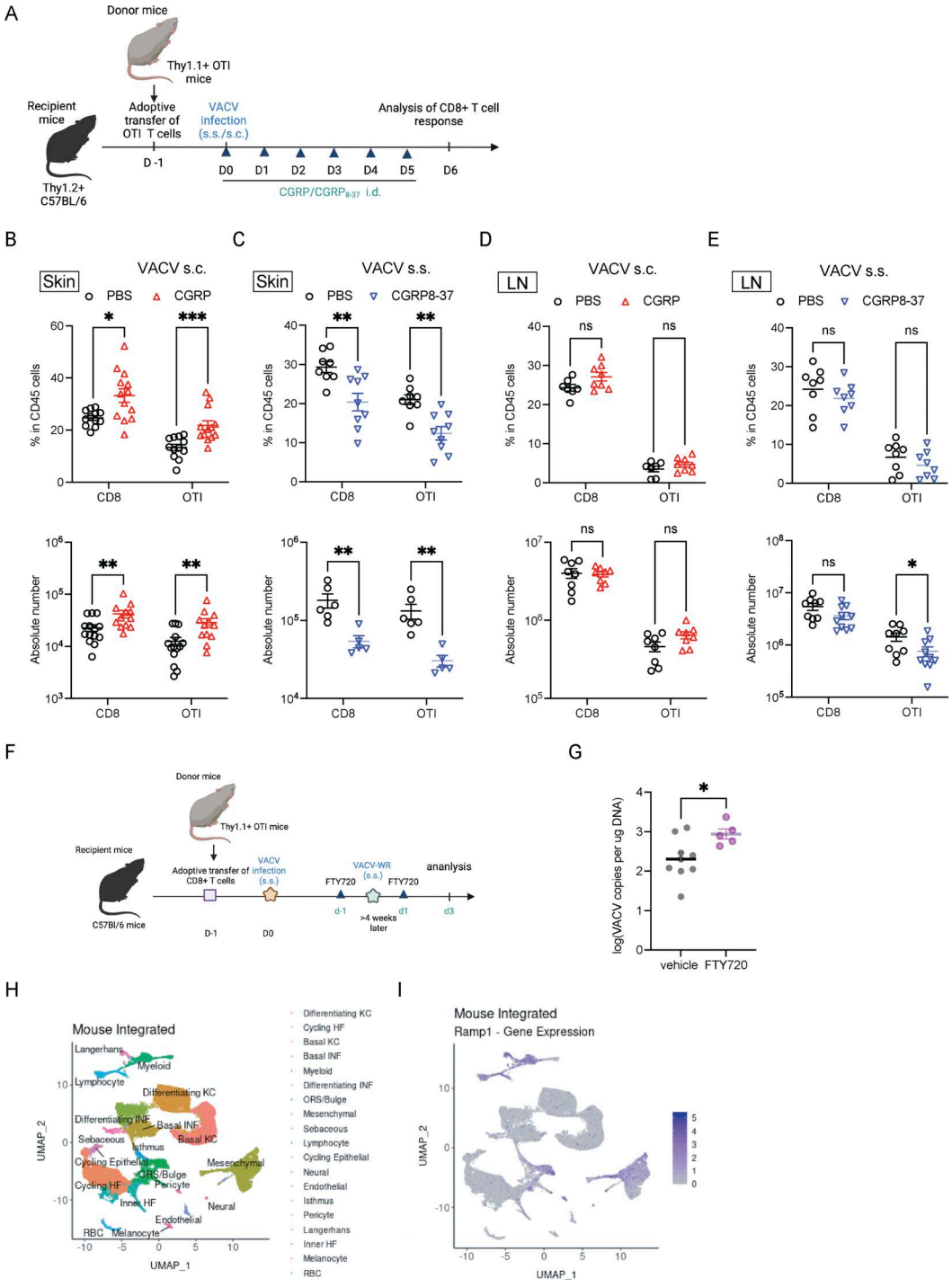

Figure S3. **Effects of CGRP signaling on CD8⁺ T cell responses and Ramp1 expression in skin cell populations. (A)** Experimental design to determine the effect of CGRPα or antagonist CGRP8-37 injection on primary effector CD8⁺ T cell response. Naïve Thy1.1⁺ OT-I cells were transferred into Thy1.2⁺ C57BL/6 mice 1 day before infection with VACV-OVA via s.c. route or s.s. Recipient mice were treated with CGRPα from day 0 to day 5 and analyzed by flow cytometry on day 6 after infection. **(B–E)** Percentages and absolute numbers of total CD8 T cells and virus-specific CD8 T cells (Thy1.1⁺ OT-I) in skin and LN were determined on day 6 in (B and D) CGRPα-treated and (C and E) CGRP8-37-treated. Data in B and D are from *n* = 8–13 mice per group pooled from two independent experiments; data in C and E are from *n* = 5–10 mice per group pooled from two independent experiments. **(F)** Experimental design to determine the effect of T_{CM} in clearing the virus. Mice were adoptively transferred with OT-I cells and immunized with VACV-OVA. >28 days later, mice were treated with FTY720 1 day before and 1 day after VACV-WR rechallenge. Skin samples were collected 3 days after VACV-WR rechallenge for quantification of viral DNA. **(G)** DNA from FTY720-treated or vehicle-treated mice was extracted for quantitative PCR to quantify the viral load of each sample. *N* = 5–8 mice per group, representative of two experiments. **(H)** Unsupervised clustering UMAPs (two-dimentional). **(I)** The relative expression of the Ramp1 gene in different skin cell populations as indicated in H. Adapted from Human-Mouse Skin database https://rstudio-connect.hpc.mssm.edu/hmsbrowser/. Mann–Whitney test was used for statistical comparisons (B–E and G), with *P < 0.05, **P < 0.01, ***P < 0.001, and "ns" indicating not significant. Error bars represent mean ± SEM. **(A and F)** Figure adapted from an image created in BioRender.

Downloaded from rupress.org/jem/article-pdf/223/12/e20261215/2044247/jem_20261215.pdf by University of California Irvine user on 16 November 2026

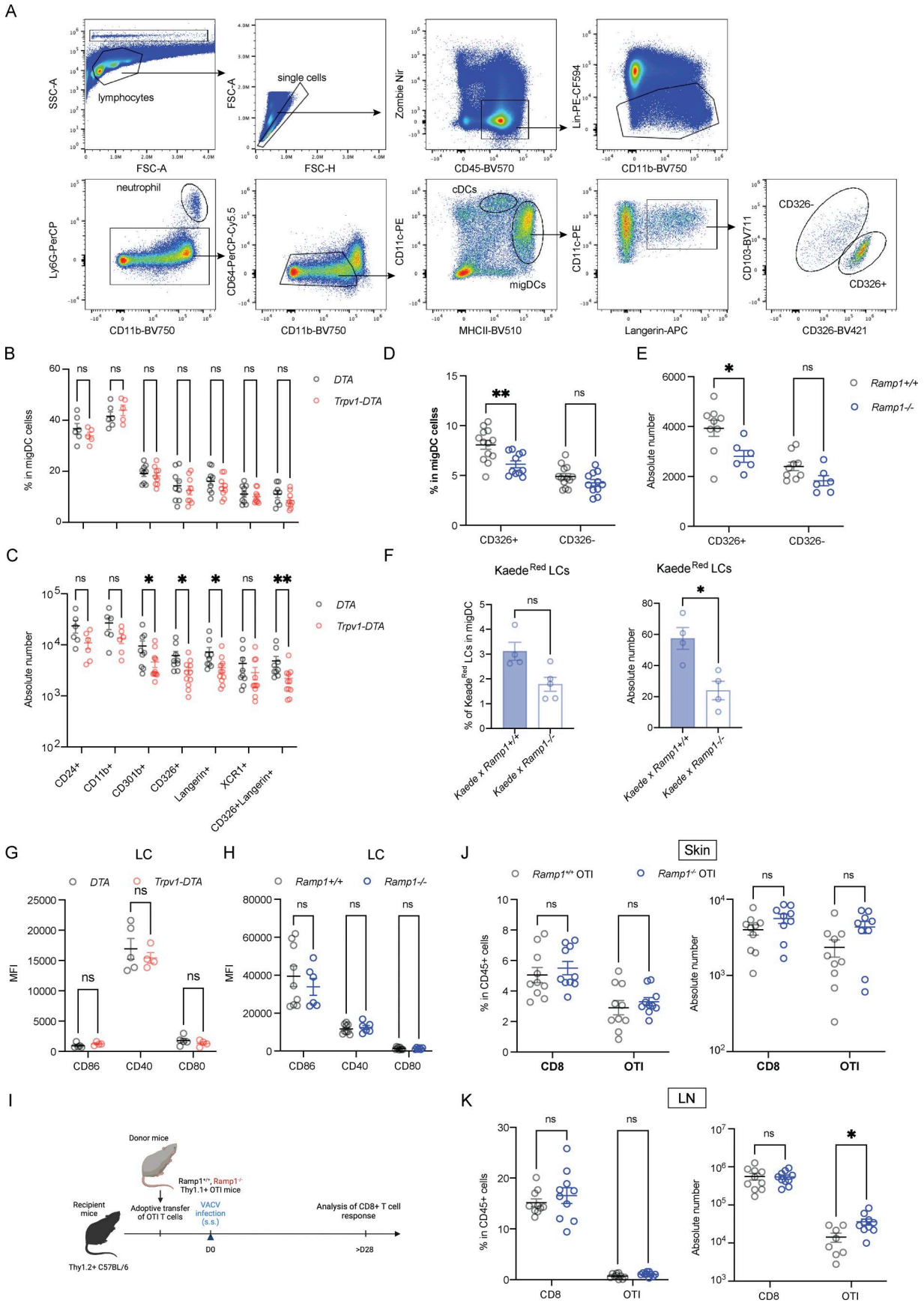

Downloaded from rupress.org/jem/article-pdf/223/12/e20261215/2044247/jem_20261215.pdf by University of California Irvine user on 16 November 2026

Figure S4. **Effects of CGRP-RAMP1 signaling on LCs and CD8⁺ T cells. (A)** Representative gating strategy used for flow cytometry is shown using dLNs from WT mice 3 days after infection with VACV virus. **(B and C)** Percentages (B) and absolute numbers (C) of migDC subsets as indicated in the graph in the dLNs of *DTA* and *Trpv1-DTA* mice 72 h after VACV-GFP s.s. *N* = 6–9 mice per group pooled from two independent experiments. **(D and E)** Percentages (D) and absolute numbers (E) of two migDC subsets: Langerin⁺CD103⁻CD326⁺ (CD326⁺) and Langerin⁺CD103⁺CD326⁻ (CD326⁻) in dLNs of *Ramp1*$^{+/+}$ and *Ramp*$^{-/-}$ 72 h p.i. with VACV s.s. *N* = 6–11 mice per group, pooled from two independent experiments. **(F)** *Kaede x Ramp1*$^{+/+}$ or *Kaede x Ramp1*$^{-/-}$ mice were photoconverted and VACV immunized. 72 h later, dLNs were collected for flow cytometry analysis. *N* = 4–5 mice per group, representative of two independent experiments. **(G)** The geometric fluorescence intensity of co-stimulatory molecules (CD40, CD80, and CD86) in migrating LCs in skin dLNs from *Ramp1*$^{+/+}$ and *Ramp*$^{-/-}$ immunized mice. *N* = 6–9 mice per group pooled from two independent experiments. **(H)** The geometric fluorescence intensity of co-stimulatory molecules (CD40, CD80, and CD86) in migrating LCs in skin dLNs from *DTA*- and *Trpv1-DTA*–immunized mice. *N* = 4–5 mice per group, representative of two independent experiments. **(I)** Experimental design to determine the effect of CGRP-Ramp1 signaling from OT-I T cells on memory CD8⁺ T cell response. Naïve Thy1.1⁺ Ramp1$^{+/+}$ or Ramp1$^{-/-}$ OT-I cells were transferred into Thy1.2⁺ B6 mice 1 day before infection with VACV-OVA via s.c. or s.s. Recipient mice were treated with CGRP from day 0 to day 5 and analyzed by flow cytometry on day 28 after infection. **(J and K)** Percentages and absolute numbers of total and virus-specific CD8 T cells in the (J) skin and (K) dLN were determined at day 28 after infection from either *Ramp1*$^{+/+}$ or *Ramp1*$^{-/-}$ OT-I transferred groups. *N* = 10 mice per group, representative of two independent experiments. Multiple Mann–Whitney tests were used for statistical comparisons (B–H, J, and K), with significance denoted as *P < 0.05, **P < 0.01, and "ns" indicating not significant. Error bars represent mean ± SEM. **(I)** Figure adapted from an image created in BioRender.

Downloaded from rupress.org/jem/article-pdf/223/12/e20261215/2044247/jem_20261215.pdf by University of California Irvine user on 16 November 2026

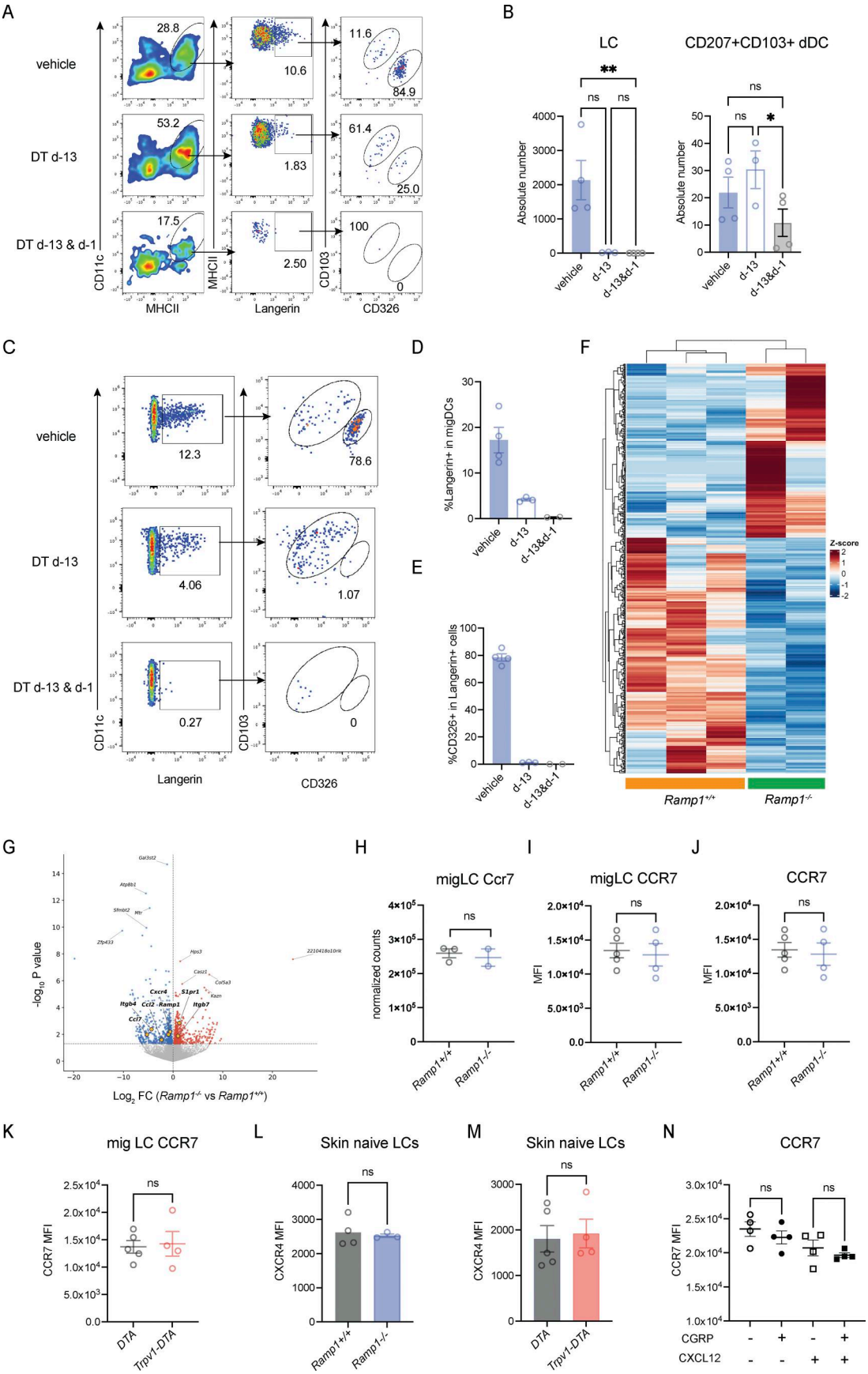

Downloaded from rupress.org/jem/article-pdf/223/12/e20261215/2044247/jem_20261215.pdf by University of California Irvine user on 16 November 2026

Figure S5. **The efficiency of Langerin$^+$ DC depletion following DT treatment. (A and B)** Langerin-DTR mice were treated with DT either 13 days prior to infection (LC-depleted group) or 13 days plus 1 day (Langerin$^+$ DC-depleted group). Skin was collected for analysis (n = 3–4 per group). **(A)** Representative flow cytometry gating strategy for analyzing skin LC$^+$ from *Langerin-DTR* mice. **(B)** Absolute number of LCs and Langerin$^+$ dDCs in the skin from different methods of DT treatment. N = 3–4 mice per group from one experiment. **(C)** Representative flow cytometry gating strategy for analyzing DCs in dLNs from *Langerin-DTR* mice. *Langerin-DTR* mice were treated with DT either 13 days prior to infection (LC-depleted group) or 13 days plus 1 day before VACV immunization (Langerin$^+$ DC-depleted group). Skin dLNs were collected 72 h after infection for analysis. **(D)** Percentage of LC$^+$ within migDC in dLNs following the different DT treatments. **(E)** Percentage of CD326$^+$ subsets within the Langerin$^+$ migratory cells. N = 2–4 mice per group from one experiment. **(F)** Heatmap of significantly differentially expressed genes (P value <0.05 and |log2FC| >1) from bulk RNA-seq of migrating LCs from dLNs of *Ramp1*$^{+/+}$ and *Ramp1*$^{-/-}$ immunized mice. **(G)** Volcano plot of significantly differentially expressed genes (P value <0.05) from bulk RNA-seq of migrating LCs from dLNs of *Ramp1*$^{+/+}$ and *Ramp1*$^{-/-}$ immunized mice. **(H)** *Ccr7*-normalized counts in Langerin$^+$CD326$^+$ migrating DCs from dLNs of *Ramp1*$^{+/+}$ and *Ramp*$^{-/-}$ mice according to the RNA-seq analysis. **(I and J)** CCR7 expression level in (I) Langerin$^+$CD326$^+$ migrating DCs and (J) migrating Langerin$^+$ dDCs from dLNs of *Ramp1*$^{+/+}$ and *Ramp*$^{-/-}$ mice. **(K)** CCR7 expression level in migrating LCs from *DTA* and *Trpv1-DTA* mice from flow cytometry analysis. **(L and M)** Skin LCs at steady state were analyzed by flow cytometry for CXCR4 expression level from (L) *Ramp1*$^{-/-}$ and *Ramp1*$^{+/+}$ and (M) *Trpv1-DTA* and *DTA* mice. N = 3–5 mice per group, representative of two independent experiments. **(N)** CCR7 expression level of migrated LCs in the transwell system treated with CXCL12 and/or CGRP ex vivo. N = 4 per group, representative of two independent experiments. One-way ANOVA (B), Mann–Whitney test (H–L), and multiple Mann–Whitney tests (M) were used for statistical comparisons, with significance denoted as *P < 0.05, **P < 0.01, and "ns" indicating not significant. Error bars represent mean ± SEM.

Downloaded from rupress.org/jem/article-pdf/223/12/e20261215/2044247/jem_20261215.pdf by University of California Irvine user on 16 November 2026

Provided online is Table S1. Table S1 shows bulk RNA-sequencing data from migratory Langerhans cells isolated from immunized mice.

Downloaded from rupress.org/jem/article-pdf/223/12/e20261215/2044247/jem_20261215.pdf by University of California Irvine user on 16 November 2026